# DOMUS Testing – Additional Validations and Verifications

**DOMUS – PROCEL EDIFICA Version Beta**

May 2011

Prepared for:

ELETROBRÁS/APC-PUCPR (Grant # ECV 283/2008)

Prepared by:


M.O. Abadie

Thermal Systems Laboratory (LST), Pontifical Catholic University of Paraná (PUCPR) , Rua Imaculada Conceicão, 1155 Curitiba, PR 80215-901, Brazil.
http://www2.pucpr.br/


Coordinated by: Prof. Nathan Mendes

**Preliminary Notes:**

This report is based upon work supported by ELETROBRÁS/APC-PUCPR in the frame of the research project “DOMUS – Software for Supporting the National Building Energy Efficiency Code: Validation, Research and Dissemination” (Grant # ECV 283/2008).

# Table of Contents

# 1 TEST OBJECTIVES AND OVERVIEW

## 1.1 Introduction

This report describes the additional validations and verifications performed to test the capabilities of DOMUS to treat heat and mass transfer problems not covered by ASHRAE 1052 – RP Toolkit "Building Fabric Analytical Tests" nor ANSI/ASHRAE Standard 140 – 2007 titled Standard Method of Test for the Evaluation of Building Energy Analysis Computer Programs. The present report has been structured in 2 main parts: the first one is devoted to moisture transport inside the porous materials employed in the envelop structure and its effect on room air humidity levels and building energy consumption and the second one is dedicated to airflow through large external apertures as windows and doors which evaluation is of great importance when natural ventilation takes place.

Table 1-1 presents the different cases treated in the present report. The first case called "HAMSTAD – Analytical Benchmark n°2" regards the drying of a concrete slab and DOMUS predictions are compared to the analytical solution. The second test called "ANNEX 41 Subtask 1 – Common Exercise 1A and 1B" aims at predicting the relative humidity variation of a room air when subjected to a periodic vapor release considering or not the presence of the envelop porous materials under isothermal conditions. The third case, "ANNEX 41 Subtask 1 – Common Exercise 3 (Whole building heat and moisture analysis)", is related to the variations of the temperature, relative humidity and heating energy of two in-situ real-sized rooms that present different amount of porous material. The last moisture-related comparison, "MBV Experiment – PUCPR", regards the variation of the moisture inside the porous material of a test-cell located in temperature and relative humidity-controlled chamber. The author wants to inform the reader that DOMUS is based on the UMIDUS model to calculate heat and moisture transport in porous materials. UMIDUS has been validated in several published papers whose results are not presented here as they can be easily found in the literature in Mendes *et al.* (1999, 2000, 2002a, 2002b, 2003), Santos *et al.* (2003) and Abadie and Mendes (2006a) to cite a few. The first case of the Natural Ventilation problems "CP – Pressure Coefficient Evaluation" aims at verifying the implementation in DOMUS of a model designed to calculate the pressure coefficients at the external surfaces of the envelop. Those coefficients are of great importance to naturally ventilated buildings as they are used to define the boundary conditions, i.e. the pressure at the external openings, needed to determine the airflow rates through the cracks, windows and doors. The second validation "NATVENT 1 – Wind-Tunnel Experiments" aims at comparing the different models implemented in DOMUS to the cases of cross- and single-sided ventilation using the results of measurements performed in a real-sized room located in a wind tunnel. To finish, the case "NATVENT 2 – On-Site Experiments" aims at comparing the predictions of DOMUS to an in-situ experiment about single sided ventilation.

Table 1-1: Additional Verifications and Validations of DOMUS.

| | Name |
|---|---|
| Moisture | HAMSTAD – Analytical Benchmark n°2 |
| | ANNEX 41 Subtask 1 – Common Exercise 1A and 1B |
| | ANNEX 41 Subtask 1 – Common Exercise 3 (Whole building heat and moisture analysis) |
| | MBV Experiment – PUCPR |
| Natural Ventilation through Large Openings | CP – Pressure Coefficient Evaluation |
| | NATVENT 1 – Wind-Tunnel Experiments |
| | NATVENT 2 – On-Site Experiments |

## 1.2 HAMSTAD – Analytical Benchmark n°2

The following description is based on the original document written by Hagentoft (2002).

### 1.2.1 Introduction

The objective of this part of the HAMSTAD project was to propose a reference HAM (Heat, Air and Moisture)-document, describing the physics of heat, moisture and air transfer including the treatment of the necessary material properties, boundary, initial and contact conditions. Five benchmark cases are defined and several numerical solutions for these are provided in Hagentoft (2002). The present validation concerns Benchmark n°2.

### 1.2.2 Description

A homogeneous layer is analyzed under isothermal conditions in one dimension. The layer is initially in moisture balance with the ambient air, having constant relative humidity. At time zero there is a sudden change in the relative humidity of the surrounding air. The structure is perfectly airtight (Figure 1-1).

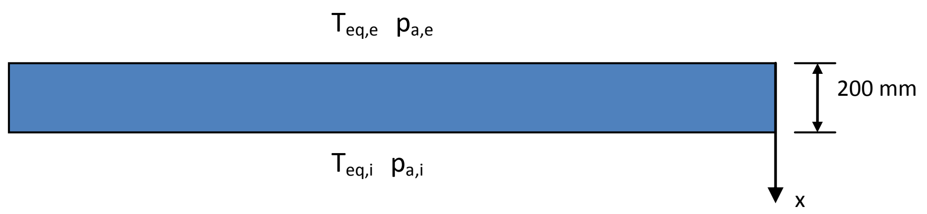


Figure 1-1: Illustration of the validation test case.

The case is isothermal with decoupled thermal and moisture processes. The latent heat of evaporation is $l_{lv} = 56.8\,J/kg$.

The material has the following properties:

1. Sorption isotherm: $w = \frac{116}{\left(1-\frac{1}{0.118}ln(\phi)\right)^{0.869}}$ kg/m$^3$
2. Vapor diffusion: $\delta_p = 1.0 \times 10^{-15}$ s
3. Moisture diffusivity: $D_w = 6.0 \times 10^{-10}$m$^2$/s
4. Thermal conductivity: $\lambda = 0.15$ W/(m.K)
5. Specific heat capacity: $c_p = 800$ J/(kg.K)
6. Density: $\rho_0 = 525$ kg/m$^3$

The thickness of the layer is 200 mm.

### 1.2.3 Boundary conditions

The equivalent temperatures that account for both ambient air temperature and radiation exchange are the same $T_{eq,e}$=20 °C, $T_{eq,i}$=20 °C.

An instant drop of air relative humidity to $\phi_{a,e}(t) = 45\%$ on exterior side and to $\phi_{a,e}(t) = 65\%$ on the interior side, i.e.:

$p_{a,e}(t) = 0.45 \times p_s(20°C)$ and $p_{a,i}(t) = 0.65 \times p_s(20°C)$ for $t > 0$

where, $p_s$, is the partial pressure at saturation (Pa).

There is no air pressure difference between the two sides of the layer (no air transport through the layer).

The surface transfer coefficients are: $\alpha_{e,e}$ = 25 W/m$^2$K, $\alpha_{e,i}$ = 25 W/m$^2$K, $\beta_{p,e}$ = 1.0×10$^{-3}$ s/m , $\beta_{p,i}$ =1.0×10$^{-3}$ s/m

The initial conditions are: w= 84.7687 kg/m$^3$ (RH =95%), T=20 °C.

### 1.2.4 Output

The total simulation time is 1000 hours. Results have to present the cross-sectional distribution of moisture content w (kg/m$^3$) at 100, 300 and 1000 hours.

## 1.3 ANNEX 41 Subtask 1 – Common Exercise 1A and 1B

The following description is partly based on the document written by Rode *et al.* (2005).

### 1.3.1 Introduction

The intention of this common exercise is to simulate a fictive room where moisture production periodically takes place. The effects of the porous material of the wall on the level of relative humidity of the room air are studied here.

### 1.3.2 Description

Two basic cases of moisture perturbation (Figure 3) are studied here. Both configurations are isothermal (T = 20°C). There is a periodic moisture perturbation induced by the presence of an internal moisture gain ($G_0$ = 0.5 kg/h) between 9:00 and 17:00 every day. There are no moisture gains outside these hours. External air enters the room at a constant rate of 0.5 ach. Outside and initial indoor vapor concentrations are set to $c_0$= 5.22 g.m-3 (= 30 % of relative humidity at 20 °C). These are also the initial conditions of the material. The external wall surface is impermeable. Case 1A considers an impermeable internal wall surface ($\beta$=0) while Case 2A includes the moisture transfer between the zone air and the envelop ($\beta \neq 0$). A semi-analytical solution has been provided by Bednar and Hagentoft (2005). For both cases, the wall is made up of 0.15 m aerated concrete ($\rho$ = 650 kg/m$^3$). The vapor permeability is $\delta p = 3.0\times10^{-11}$ kg/m.s.Pa and the moisture capacity of the material is $\zeta$ = 0.0661 kg/m$^3$.

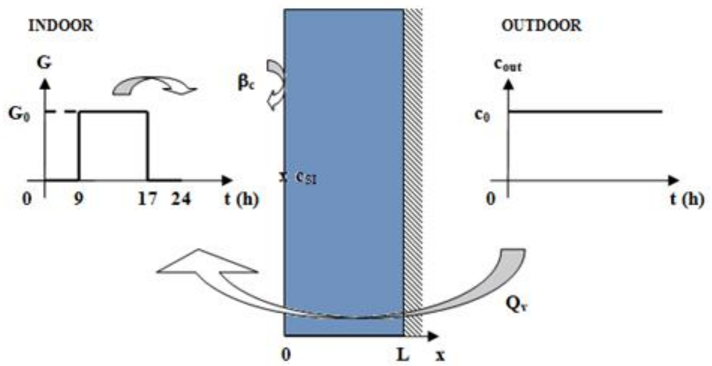


Figure 1-2: Moisture perturbations of tests 1A ($\beta$=0) and 1B ($\beta \neq 0$).

### 1.3.3 Outputs

The required outputs are the relative humidity variations versus time for cases 1A (no porous material) and 1B (presence of a porous material).

## 1.4 Introduction ANNEX 41 Subtask 1 – Common Exercise 3 (Whole building heat and moisture analysis)

The following description is based on the original document written by Lenz and Holm (2005).

### 1.4.1 Introduction

The intention of this common exercise is to simulate two real test rooms which are located at the outdoor testing site of the Fraunhofer-Institute of building physics in Holzkirchen. The results of the measurements show the influence of different materials in comparison to the relative humidity in the rooms. In the reference room a standard common used gypsum plaster with a latex paint (sd = 0,15 m) is used. The walls and the ceiling of the test room are fully coated with aluminium foil. For the experiments the test materials can be attached to the walls and ceiling of the room.

### 1.4.2 Description

The tests in the rooms were made in the following three steps:

1. Reference room - Test room only with aluminium foil
2. Reference room - Test room with gypsum boards on the walls
3. Reference room - Test room with gypsum boards on the walls and the ceiling

Figure 1-3 presents the ground plan of the two test rooms. Dimensions of the room are presented in Figure 1-4.

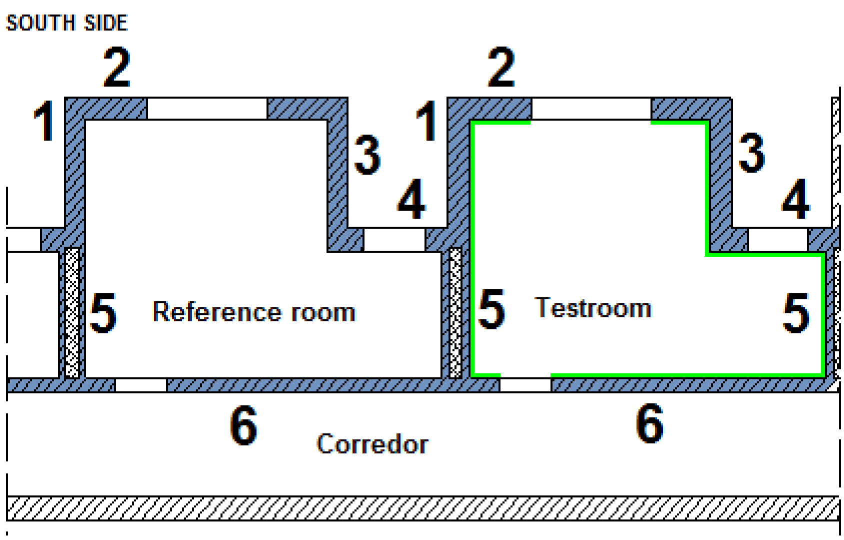


Figure 1-3: Ground plan of the test rooms (left: Reference room with gypsum plaster and latex paint; right: Test room with aluminium foil).

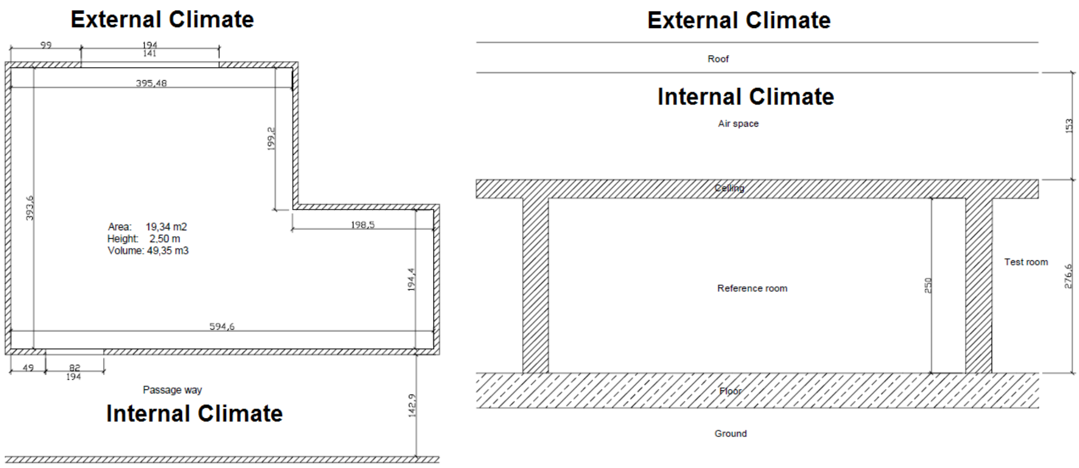


Figure 1-4: Dimensions of the test rooms (in cm).

### 1.4.3 Material specifications

Table 1-3 to Table 1-7 present the material specifications of the vertical walls (n° 1 to 6 in Figure 1-3), the ceiling and the floor. The moisture-dependent thermal conductivity of the insulation material is given by Table 1-2. Table 1-8 presents the material properties for the round-robin test (gypsum board).

Table 1-2: Thermal conductivity of mineral wool, moisture-dependent.

| Water content (kg/m³) | Thermal conductivity (W/mK) |
|---|---|
| 0 | 0.04 |
| 10 | 0.04 |
| 20 | 0.041 |
| 50 | 0.043 |
| 100 | 0.049 |
| 200 | 0.07 |
| 300 | 0.1 |
| 400 | 0.15 |
| 500 | 0.2 |
| 600 | 0.27 |
| 700 | 0.35 |
| 800 | 0.44 |
| 900 | 0.55 |
| 950 | 0.6 |

### 1.4.4 Window and door specifications

The window is included in the southern wall. It is a double-glazed window with an U-value of 1.1 W/m²K and a dimension of 1.41 x 1.94 m². During the tests a wool blanket was situated in front of the window on the outside in order to exclude any solar radiation into the rooms. Therefore for the calculations only the U-value is important. The doors from the passage way to the rooms have 5 cm polystyrene on the inside and the size of it is 1.94 x 0.82 m².

### 1.4.5 Heating, moisture load and ventilation data

The temperatures in the rooms are controlled to 20±2°C with the use of a small radiator. The required energy was recorded. The moisture production in both test rooms corresponds to a normal four person household and is converted to the test rooms. In the rooms the moisture production is 2.4 kg/d. Figure 1-5presents the selected diurnal moisture production pattern. The permanently present basic humidity production of 25 g/h is due to e.g. plants or pets. In the early morning hours between 6 am and 8 am, this value is increased to a peak level of 400 g/h in order to simulate human activities, like having a shower and washing. Subsequently, the moisture production will drop back to the basic rate of production 25 g/h. In the late afternoon the moisture production will increase again to a moderate level (200 g/h) until the evening hours (4 pm until 10 pm) which represents certain activities like cooking, cleaning or doing the laundry.

A ventilation system is installed in both rooms providing a constant air change. The air change rates during operation of the ventilation system were determined by tracer gas measurements. The air change rate for the reference room is n = 0.63 $h^{-1}$ and for the test room is n = 0.66 $h^{-1}$.

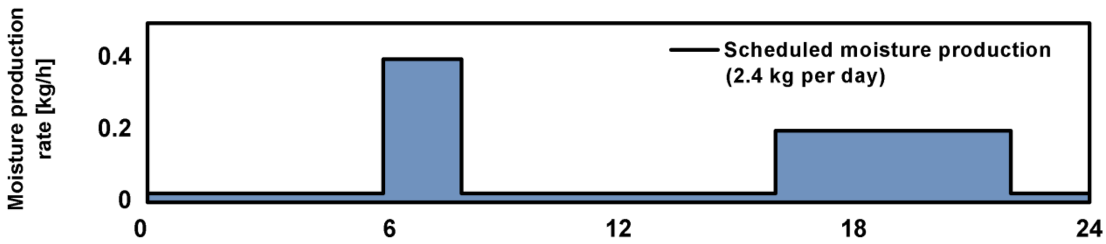


Figure 1-5: Moisture production in the test rooms.

### 1.4.6 Radiation and surface coefficients of heat transfer

Long-wave emissivity and short-wave absorption coefficients are equal to 0.9 and 0.4, respectively, for all surfaces (internal and external). The convective heat transfer coefficients are set to 8 W/m²K for internal surfaces, to 18 W/m²K for external ones and 100 W/m²K for the external surface of the floor.

### 1.4.7 Boundary conditions

The boundary conditions around the rooms are different (see Figure 1-4). On the south side, it is external climate zone and on the north side and over the ceiling there is internal climate. The passage way and over the ceiling it is an unheated area. On the left and right side of the rooms the climate conditions are 20°C and 50 % RH. But for the calculations the climate in the next rooms are not very important because the indoor walls are thermally decoupled. The boundary conditions for the ground are on the average 2°C.

### 1.4.8 Simulated cases

The flowing three configurations have been tested:

1. Step 1: Reference room - <u>Test room only with aluminium foil</u>
   During the first test stage no material was attached to the walls in the test room and measurements run from 2005-01-17 to 2005-02-02. This test shows the differences between the reference room and the test room with aluminium foil where no sorption effects were possible.

2. Step 2: Reference room - Test room with gypsum boards on the walls
   In the second step, gypsum boards were attached on top of the walls with aluminium foil inside the test room which accord the area of the walls (50 m²), this experiment run from 2005-02-14 to 2005-03-20. For the test, gypsum boards without paint were used.
3. Step 3: Reference room - Test room with gypsum boards on the walls and roof
   For this experiment additional (65 m²) gypsum boards were installed inside the room with aluminium foil on the top of the walls and the ceiling. The test was carried out from 2005-03-27 to 2005-04-22. For the test, gypsum boards without paint were inserted.

### 1.4.9 Outputs

The following outputs were required to all participants of the round-robin test:

1. Hourly averaged air temperatures of the air in both rooms (constant and equals to 20°C),
2. Hourly average relative humidity of the air in both rooms, and
3. Energy in order to keep the constant temperature.

Simulations have to be run as long as it is necessary to reach quasi-steady conditions.

Table 1-3: Material specifications – Wall 1 to 4.

| Materials | Thickness (m) | Density (kg/m³) | Porosity (m³/m³) | $c_p$ (J/kgK) | lambda _dry (W/mK) | µ_dry (-) | W_80 (kg/m³) | W_f (kg/m³) | A_f (kg/m²√s) |
|---|---|---|---|---|---|---|---|---|---|
| Outdoor surface | | | | | | | | | |
| Mineral plaster | 0.005 | 1900 | 0.24 | 850 | 0.8 | 25 | 45 | 210 | 0.002 |
| Polystyrene | 0.07 | 30 | 0.95 | 1500 | 0.04 | 50 | 0 | 0 | 0 |
| Mineral plaster | 0.015 | 1900 | 0.24 | 850 | 0.8 | 25 | 45 | 210 | 0.002 |
| Brick | 0.24 | 1650 | 0.4 | 850 | 0.6 | 9.5 | 9 | 370 | 0.4 |
| Old inside plaster | 0.02 | 1721 | 0.31 | 850 | 0.2 | 13 | 1.8 | 264 | 0.3 |
| Gypsum plaster | 0.01 | 850 | 0.65 | 850 | 0.2 | 8.3 | 6.3 | 400 | 0.3 |
| Aluminium foil* | $5\times10^{-5}$ | | | | | 10000 | 0 | 0 | 0 |

*only in the right test room.

Table 1-4: Material specifications – Wall 5.

| Materials | Thickness (m) | Density (kg/m³) | Porosity (m³/m³) | $c_p$ (J/kgK) | lambda _dry (W/mK) | µ_dry (-) | W_80 (kg/m³) | W_f (kg/m³) | A_f (kg/m²√s) |
|---|---|---|---|---|---|---|---|---|---|
| Outdoor surface | | | | | | | | | |
| Gypsum plaster | 0.01 | 850 | 0.65 | 850 | 0.2 | 9 | 6 | 400 | 0.3 |
| Solid brick | 0.115 | 1650 | 0.4 | 850 | 0.6 | 9.5 | 9 | 370 | 0.4 |
| Mineralwool[1)] | 0.10 | 60 | 0.95 | 850 | 0.04 | 1.3 | 0 | 0 | 0 |
| Solid brick | 0.115 | 1650 | 0.4 | 850 | 0.6 | 9.5 | 9 | 370 | 0.4 |
| Gypsum | 0.01 | 850 | 0.65 | 850 | 0.2 | 9 | 6 | 400 | 0.3 |

| | | | | | | | | | |
|---|---|---|---|---|---|---|---|---|---|
| plaster | | | | | | | | | |
| Aluminium foil* | $5\times10^{-5}$ | | | | | 10000 | 0 | 0 | 0 |

*only in the right test room.

Table 1-5: Material specifications – Wall 6.

| **Materials** | **Thickness (m)** | **Density (kg/m³)** | **Porosity (m³/m³)** | **$c_p$ (J/kgK)** | **lambda _dry (W/mK)** | **µ_dry (-)** | **W_80 (kg/m³)** | **W_f (kg/m³)** | **A_f (kg/m²√s)** |
|---|---|---|---|---|---|---|---|---|---|
| Outdoor surface | | | | | | | | | |
| Gypsum board | 0.0125 | 850 | 0.65 | 870 | 0.16 | 6 | 35 | 400 | 0.3 |
| Polystyrene | 0.05 | 30 | 0.95 | 1500 | 0.04 | 50 | 0 | 0 | 0 |
| Lime silica brick | 0.175 | 1900 | 0.29 | 850 | 1 | 28 | 25 | 250 | 0.045 |
| Gypsum plaster | 0.015 | 850 | 0.65 | 850 | 0.2 | 9 | 6 | 400 | 0.3 |
| Aluminium foil* | $5\times10^{-5}$ | | | | | 10000 | 0 | 0 | 0 |

*only in the right test room.

Table 1-6: Material specifications – Ceiling.

| **Materials** | **Thickness (m)** | **Density (kg/m³)** | **Porosity (m³/m³)** | **$c_p$ (J/kgK)** | **lambda _dry (W/mK)** | **µ_dry (-)** | **W_80 (kg/m³)** | **W_f (kg/m³)** | **A_f (kg/m²√s)** |
|---|---|---|---|---|---|---|---|---|---|
| Outdoor surface | | | | | | | | | |
| Wood | 0.025 | 400 | 0.73 | 1500 | 0.09 | 200 | 60 | 575 | 0 |
| Concrete screed | 0.05 | 1950 | 0.18 | 850 | 1.6 | 75 | 38 | 155 | |
| Polystyrene | 0.2 | 30 | 0.95 | 1500 | 0.04 | 50 | 0 | 0 | 0 |
| Concrete | 0.175 | 2300 | 0.18 | 850 | 1.6 | 180 | 85 | 150 | 0.02 |
| Gypsum plaster | 0.015 | 850 | 0.65 | 850 | 0.2 | 9 | 6 | 400 | 0.3 |

| | | | | | | | | | |
|---|---|---|---|---|---|---|---|---|---|
| Aluminium foil* | $5\times10^{-5}$ | | | | | 10000 | 0 | 0 | 0 |

*only in the right test room.

Table 1-7: Material specifications – Floor.

| **Materials** | **Thickness (m)** | **Density (kg/m³)** | **Porosity (m³/m³)** | **$c_p$ (J/kgK)** | **lambda _dry (W/mK)** | **μ_dry (-)** | **W_80 (kg/m³)** | **W_f (kg/m³)** | **A_f (kg/m²√s)** |
|---|---|---|---|---|---|---|---|---|---|
| Outdoor surface | | | | | | | | | |
| Concrete | 0.25 | 2300 | 0.18 | 850 | 1.6 | 180 | 85 | 150 | 0.02 |
| Polystyrene | 0.2 | 30 | 0.95 | 1500 | 0.04 | 50 | 0 | 0 | 0 |
| Concrete screed | 0.05 | 1950 | 0.18 | 850 | 1.6 | 75 | 38 | 155 | |
| PVC linoleum | 0.003 | 1000 | 0.16 | 1500 | 0.16 | 15000 | 0 | 0 | 0 |

Table 1-8: Material specifications – Gypsum board.

| **Materials** | **Thickness (m)** | **Density (kg/m³)** | **Porosity (m³/m³)** | **$c_p$ (J/kgK)** | **lambda _dry (W/mK)** | **μ_dry (-)** | **W_80 (kg/m³)** | **W_f (kg/m³)** | **A_f (kg/m²√s)** |
|---|---|---|---|---|---|---|---|---|---|
| Gypsum board | 0.0125 | 710 | 0.65 | 850 | 0.31* | 8 | 9.5 | 400 | 0.3 |

*Data Specification from producer

## 1.5 MBV – PUCPR

The following description is based on the original document written by Meissner *et al.* (2010).

### 1.5.1 Introduction

The objective of this experimental work was to present a full-scale experimental apparatus to evaluate the hygroscopic inertia of porous building materials, whose principle is based on measurements of the changes in mass of a porous material when its neighboring environment is subjected to daily cyclic variation of relative humidity. Results in terms of the moisture buffer value index (MBV) for a light weight wood construction material are also presented and discussed, considering two sample sizes: a cubic cell with 24 $m^2$ of mass exchange surface area and a smaller one with a circular exposed area of approximately 0.08 $m^2$. This experiment has been designed at the Thermal Systems Laboratory (LST) of Pontifical Catholic University of Paraná (PUCPR).

### 1.5.2 Description

The principle of the proposed moisture buffer capacity apparatus is to measure the changes in mass of a porous material when its neighboring environment is subjected to daily cyclic variation of relative humidity. Basically, the whole facility is composed of a 8 $m^3$ cubic test-cell made of the hygroscopic material to be tested, an air tunnel to provide controlled psychrometric conditions within the test-cell, and two climate chambers: one to supply pre-conditioned air at the entrance of the handling air tunnel (Chamber 1) and the other to simulate the external environment for the built-in test-cell (Chamber 2).

The internal volume of chamber 1 is 25.11 $m^3$ and its temperature and relativity humidity operation ranges are respectively 0 to 60ºC ±0.1ºC and 30 to 70% ±5%RH, while the internal volume of chamber 2 is 40.66 $m^3$ and its temperature and relativity humidity operation ranges are 25 to 70ºC ±0.1ºC and 30 to 99%RH ±1%RH, respectively.

The built-in test-cell is composed of two wood structures. One of them supports all sensors and the 6 square-shaped sheets of 2 m edge of the porous material to be tested, which are placed on a frame to form an 8 $m^3$ cubic cell with approximately 24 $m^2$ of heat and mass transfer surface area.

The second wood structure maintains the assembly (cubic frame + specimen sheets) 0.5 m above the chamber floor to provide air circulation around all specimen sheets, and also supports the four load cells that measures changes in mass of the porous material caused by the RH variations in the neighboring environment. An illustration of both wood structures is shown in Figure 1-6.

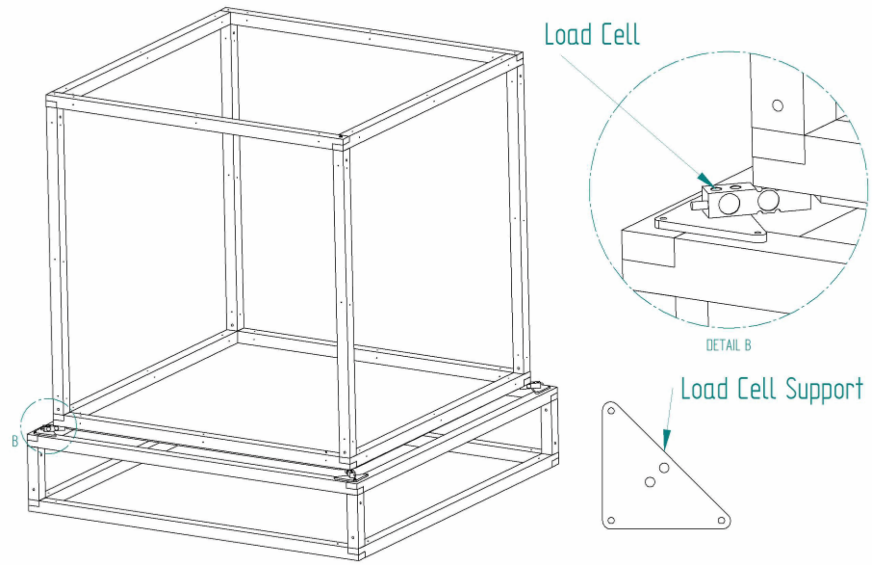


Figure 1-6: Wood structures of the test cell.

As the structure that supports the specimen sheets is also made of a hygroscopic material, it was carefully varnished to avoid its interference on the determination of the moisture buffer capacity of the material under analysis.

The air tunnel was conceived to provide specific psychrometric conditions at the supply opening of the test-cell. It takes cold dry air from Chamber 1 and regulates the temperature and relative humidity of the air to the set-point condition using both electrical resistance and an electronic controlled water vapor generator, while the mass flow rate is adjusted by a variable speed radial fan. The air tunnel is connected to the test-cell using a flexible circular duct (D=300 mm) insulated to minimize any heat transfer with the surrounding environment, which covers a straight rigid duct of 3 m long that guarantees a hidrodynamically developed airflow at the entrance of the test-cell. The three variables, temperature, relative humidity and mass flow rate, are automatic controlled using PID control with respect to a T-Type thermocouple and a RH transmitter located at the inlet opening of the test-cell and to a velocity sensor placed in the center of the straight rigid duct at 2.5 m from its beginning. Figure 1-7 shows a sketch of the whole experimental set-up.

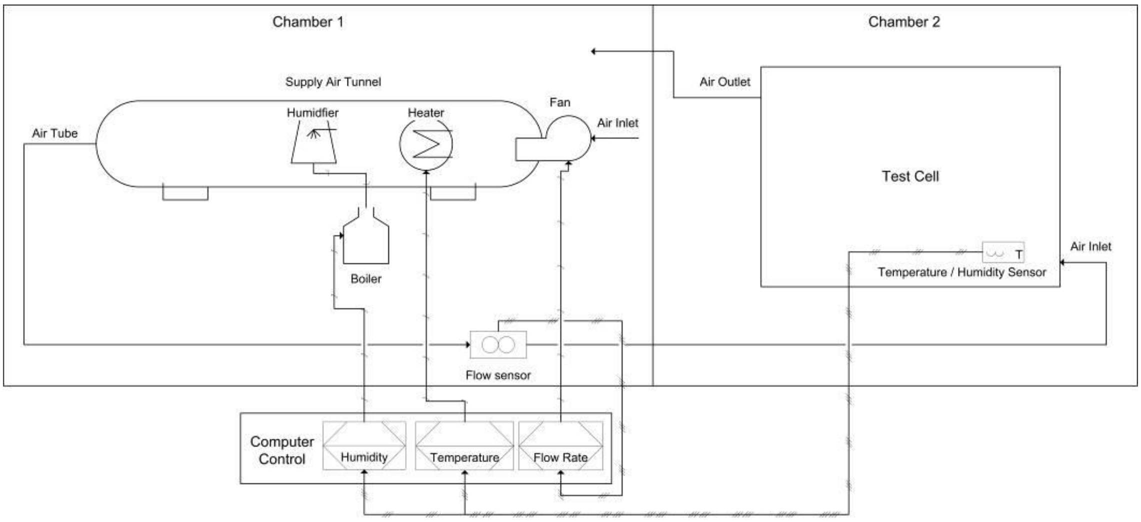


Figure 1-7: Sketch of the whole experimental set-up.

It can be seen in this figure that the air is supplied horizontally by an opening located at the lower right corner of the test-cell and is exhausted through an opening on the upper left corner on the opposite side. Both openings are circular (internal diameter of 7.87cm).

As the internal volume of the test-cell is quite significant (around 8 $m^3$), temperature, relative humidity and air velocity were monitored in different positions within the test-cell to evaluate the heterogeneity of its indoor environment, as illustrated in Figure 1-8.

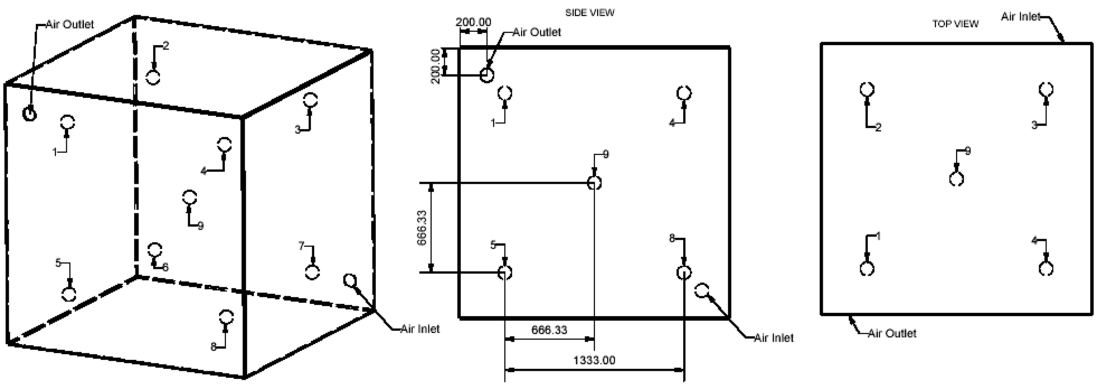


Figure 1-8: Positions of the sensors of temperature, relative humidity and velocity inside the test-cell.

### 1.5.3 Measurement protocol

The moisture buffer capacity tests were run based on the test protocol developed in the NORDTEST project (Rode, 2005) to determine the practical moisture buffer value index ($MBV_{practical}$). In this protocol, an asymmetric RH square wave signal is imposed to the air surrounding a sample of a porous material, while the temperature is kept constant at 23°C. In fact, the specimen is exposed to a high RH level (75%) along 8h, followed by a 16h period of low RH level (33%). The exposure is repeated in cycles until quasi-steady equilibrium is achieved, i.e., the amount of moisture uptake or release by the porous material should not vary more than 5% in three consecutive cycles. The mean of the average between the measured amount of water exchanged during the uptake and the release period in the quasi-steady equilibrium ($\Delta$m) per exposed surface area of the material (S) and per %RH variation ($\Delta$%RH) gives the $MBV_{practical}$ index (kg/m$^2$%RH), as expressed in Eq. (1).

$$MBV_{practical} = \frac{\Delta m}{S \times \Delta\% RH} \tag{1}$$

According to the $MBV_{practical}$ protocol, the airflow around the material under analysis should reproduce a normal indoor environment with air velocities about 0.10 ± 0.05 m.s$^{-1}$, corresponding to a surface film resistance of 5.0x10$^7$ m$^2$.s.Pa.kg$^{-1}$. This has been achieved maintaining an airflow rate equivalent to about 2.5 ACH.

### 1.5.4 Outputs

The following outputs are required for comparison with the experimental results:

1. Evolution of the temperature and relative humidity of the room air with time,
2. Change of mass of the porous material, and
3. MBV value.

## 1.6 CP – Pressure Coefficient Evaluation

### 1.6.1 Introduction

CPCALC+ is a program for calculating wind pressure coefficients on the envelope of a building for airflow modeling, developed within the European Research Program PASCOOL (Passive Cooling of Buildings) of the Commission of the European Communities, Directorate General for Energy (Grosso, 1993; Grosso *et al.*, 1994). It has been developed at the Lawrence Berkeley Laboratory within the COMIS workshop on infiltration and ventilation (Feustel and Rayner-Hooson, 1990; Grosso, 1992), and being upgraded within the IEA-ANNEX 23 on multizone airflow modeling. A modular framework allows for upgrading CPCALC by adding subroutines related to new application configurations. CPCALC+ includes new subroutines dealing with roofs as well as a WINDOWS Visual Basic User Interface. CPCALC, and CPCALC+, were developed in order to fulfill the requirements of multizone airflow models which need a detailed evaluation of the wind pressure distribution around buildings. Scientists and professionals using this program, and who do not have the possibility to test a scale model of their building in a wind tunnel, do not need to extrapolate Cp data from tables usually yielding wall-averaged Cp values (Liddament, 1986). The present section aims at verifying the implementation of the CPCALC+ algorithm in DOMUS and at comparing its prediction to published data regarding pressure distribution around buildings

### 1.6.2 Description

CPCALC+ was developed analysing the wind tunnel data from Hussein and Lee (1980) and Akins and Cermak (1976). Each parameter, which has an effect on the pressure coefficient (Cp) was taken as independent variable while keeping the other variables constant. Variation curves for each parameter were then defined with statistical regressions. The parameters include:

1. Wind direction (Figure 1-9): 0° for wind coming from North, +90° for wind coming from East, +180° for wind coming from South and +270° for wind coming from West.
2. Wind velocity profile exponent (alpha): see Table 1-9.
3. Surrounding Building Height: averaged height of surrounding buildings.
4. Plan Area Density (pad): the Plan Area Density is a parameter related to the layout pattern of the buildings surrounding the building under examination. Wind tunnel test data show that the radius of the built area surrounding the building, and affecting the wind pressure distribution on its envelope, is inversely proportional to the plan area density. The pad has to be evaluated within a radius ranging from 10 to 25 times the height of the considered building.
5. Building dimensions: Height
6. Wall azimuth (Figure 1-10): 0° for wall facing North, +90° for wall facing East, +180° for wall facing South, and +270° for wall facing West.
7. Location of CP calculation (Figure 1-10): The origin of (0, x, z) is taken as the point located at the lower left corner of the wall looking at this wall (wall normal coming to us).
    a. Point horizontal coordinate (x),
    b. Point vertical coordinate (h),
    c. Length of the considered facade (L1),

d. Length of the facade adjacent to the considered façade (L2).

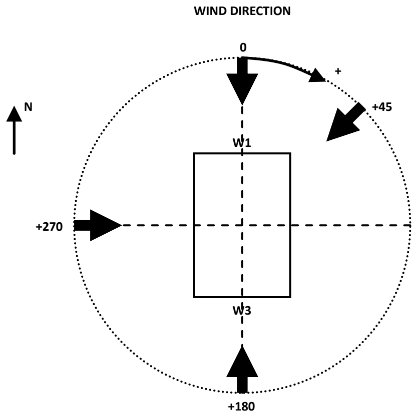


Figure 1-9: Wind direction.

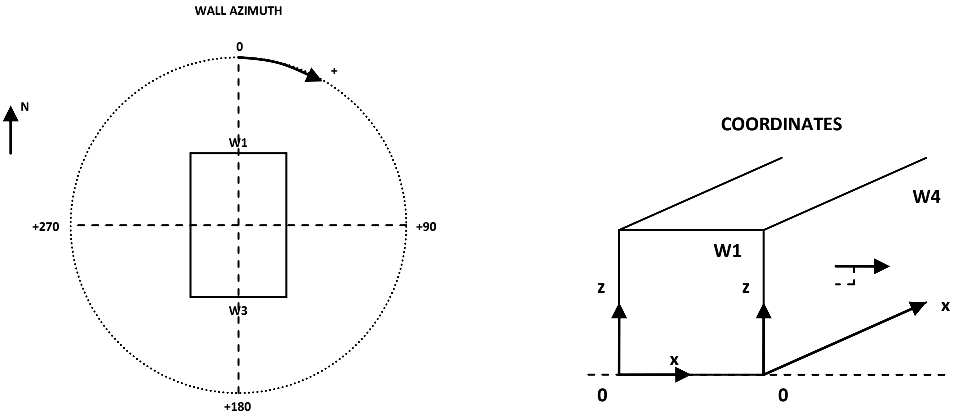


Figure 1-10: Wall azimuth and Point horizontal (x) and vertical (z) coordinates.

Table 1-9: Reference Values for the Wind Velocity Profile Exponent (alpha).

| Terrain Roughness Type | alpha |
|---|---|
| Level surfaces, surfaces of water basins, grass land | 0.10 |
| Flat open country with few, very small, and scattered obstructions | 0.14 |
| Rolling or level surfaces broken by numerous obstructions such as trees or small houses | 0.22 |
| Heterogeneous surface with obstacles larger than one story | 0.28 |
| Low density suburban areas | 0.34 |
| Medium-high density urban areas | 0.40 |
| Very high density inner city areas | 0.45 |

From those parameters, six intermediate parameters are calculated:

1. Relative Building's Height (rbh): The relative building height is the ratio of the building's height to the averaged height of surrounding buildings.
2. Frontal Aspect Ratio (far): The frontal aspect ratio is the ratio of the length of the considered facade to its height.

3. Side Aspect Ratio (sar): The side aspect ratio is the ratio of the length of the facade adjacent to the considered one, to the facade's height.
4. Point dimensionless horizontal coordinate (xl): The point dimensionless horizontal coordinate is the ratio of the point horizontal coordinate to the façade's horizontal dimension.
5. Point dimensionless vertical coordinate (zh): The point dimensionless vertical coordinate is the ratio of the point vertical coordinate to the façade's vertical (=height) dimension.
6. Wind-to-wall angle: The wind-to-wall angle is defined as the difference between the wind direction and the wall azimuth.

The Cp value is then calculated by multiplying the intermediate Cp values related to the six previous intermediate parameters.

Note that the CPCALC+ applies to rectangular-plan buildings with boundary conditions comprised in given variation ranges related to the Cp data on which the parametrical analysis was based. For each parameter, or for a combination of parameters, two levels of variation range are foreseen: the larger one is the maximum range outside of which the calculation cannot be executed; the stricter one is the confidence range, outside of which results are given but the accuracy is not assured. Table 1-10 shows the two-level variation range for the various parameters. However, no absolute values of Cp greater than 1 should be accepted, except for very high simultaneous values of the parameters pad, far and sar when the absolute Cp can reach values of 1.2-1.3.

Table 1-10: Application ranges of CPCALC+ - Vertical walls.

| | Confidence Range | | Maximum Range | |
|---|---|---|---|---|
| **Parameter** | **Constant** | **Independent Variable** | **Constant** | **Independent Variable** |
| alpha | $0.1 \le zh \le 0.9$ | $0.10 \le alpha \le 0.33$ | $0.0 \le zh \le 1.0$ | $0.10 \le alpha \le 0.45$ |
| Pad | $0.07 \le zh \le 0.93$ | $0.0 \le pad \le 50.0$ | $0.0 \le zh \le 1.0$ | $0.0 \le pad \le 50.0$ |
| Rbh | $0.07 \le zh \le 0.93$<br>$0.0 \le pad \le 25$ (*) | $0.5 \le rbh \le 4.0$ | $0.0 \le zh \le 1.0$<br>$0.0 \le pad \le 25$ (*) | $rbh \ge 0.0$ |
| Far | $0.07 \le zh \le 0.93$<br>$0.0 \le pad \le 12.5$ (*) | $0.5 \le far \le 4.0$ | $0.0 \le zh \le 1.0$<br>$0.0 \le pad \le 12.5$ (*) | $far \ge 0.0$ (#) |
| Sar | $0.07 \le zh \le 0.93$<br>$0.0 \le pad \le 12.5$ (*) | $0.5 \le sar \le 2.0$ | $0.0 \le zh \le 1.0$<br>$0.0 \le pad \le 12.5$ (*) | $sar \ge 0.0$ (#) |

(*) If RbH=1 or far=1 or sar=1 → $0.0 \le pad \le 50.0$

(#) Varying in relation to specific combination of values for far, sar, pad and position coordinates of the element.

### 1.6.3 Validations

Three validation tests have been performed to verify the prediction of the CPCALC+ algorithm implemented in DOMUS:

1. A verification step of the DOMUS Cp routine has been performed by comparison with the results presented in the original work of Grosso *et al.* (1995). Cp variations according to different parameters are presented.
2. A first validation step has been done comparing the results obtained by Wong and Chin (2002) for a more complex geometry for which the Cp values have been obtained by measurement and by the use of the CPCALC+ program (Figure 1-11).

3. A second validation has been performed comparing the Cp variation on different wall for three building shapes: a cube, a tall building, and a low building with large footprint. Comparisons were made with the wind tunnel data of Baines (1963) for a cubical building and a tall building with dimensions of 1:1:8 (length, width, height).

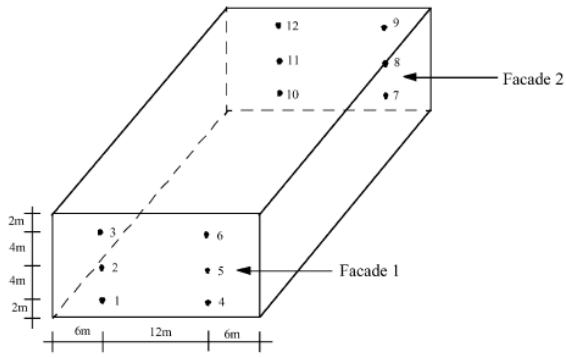


Input parameters to CpCalc+

| Parameters | Values |
|---|---|
| Wind directions (°) | 0, 45, 90, 180 |
| Building azimuth (°) | 180 |
| Wind velocity profile exponent | 0.4 |
| Plan area density (%) | 3.6 |
| Surrounding buildings' height (m) | 37 |
| Roof type | Double slope (2) |
| Roof tilt angle (°) | 24 |

Figure 1-11: Geometry and parameters (Wong and Chin, 2002) – Validation n°2.

### 1.6.4 Outputs

The following outputs are required for the verification and the two validations:

1. Verification: Cp variations according to CPCALC+ parameters such as the reference Cp, the boundary layer profile, the surrounding area density, the frontal aspect ratio and the wind angle.
2. Validations: Cp values according to the location on the building envelopes.

## 1.7 NATVENT 1 – Wind-Tunnel Experiments

The following description is based on the original document written by R.Z. Freire (2010).

### 1.7.1 Introduction

The goal of this section is to validate and compare the ventilation models implemented into DOMUS by comparing the airflow rate estimation of the cross ventilation model proposed by the British Standards (British Standards, 1999) and the single-sided ventilation models of de Gids and Phaff (1982) and Larsen (Larsen and Heiselberg, 2008) to results obtained from wind tunnel experiments. Two methodologies for evaluating the wind pressure coefficient (Cp) have also been analyzed here considering that the pressure coefficient value is necessary as an input parameter for both cross and single-sided ventilation models: the CPCALC+ algorithm (see previous section) and the use of a surface-averaged Cp value defined by Swami and Chandra (1988).

### 1.7.2 Description

The wind tunnel experiment has been carried out in a full-scale wind tunnel at the Japanese Building Research institute (BRI) by Larsen (Larsen and Heiselberg, 2008) to investigate the airflow through openings in single-sided and cross ventilation situations. The building's dimensions are 5.56 m×5.56 m×3.00 m, which means that scale effects were avoided. The opening's width and height are 0.86 m×0.15 m for both windows in the cross-ventilation case, they are positioned 0.54 m away from the right edge and 0.925 m from the top (Figure 1-12a). For the single sided case, the openings dimensions are 0.86 m×1.40 m of width and height, respectively. In this case, it is located at 0.54 m away from the right edge and 0.69 m away from the top of the building (Figure 1-12b). The internal room height is 2.4 m, the thickness of the walls is 0.10 m and the room volume is about 68.95 $m^3$.

The experiment consisted of varying the wind speed in the tunnel (1, 3 and 5 m/s) with turbulence intensity less than 5% while imposing a temperature difference of 0, 5 and 10K between the internal and external air. The temperature difference was created with four electric heaters placed inside the building. The wind speed profile created in this wind tunnel was almost uniform, which resulted in a wind profile that differs from outdoor conditions as it was not able to reproduce the atmospheric boundary layer. The building was also rotated between 0° and 345°; using either a 15° or a 30° step to obtain measurements for different wind angles. A total of 159 different cases was studied. The air-change rate was measured with the tracer gas decay method.

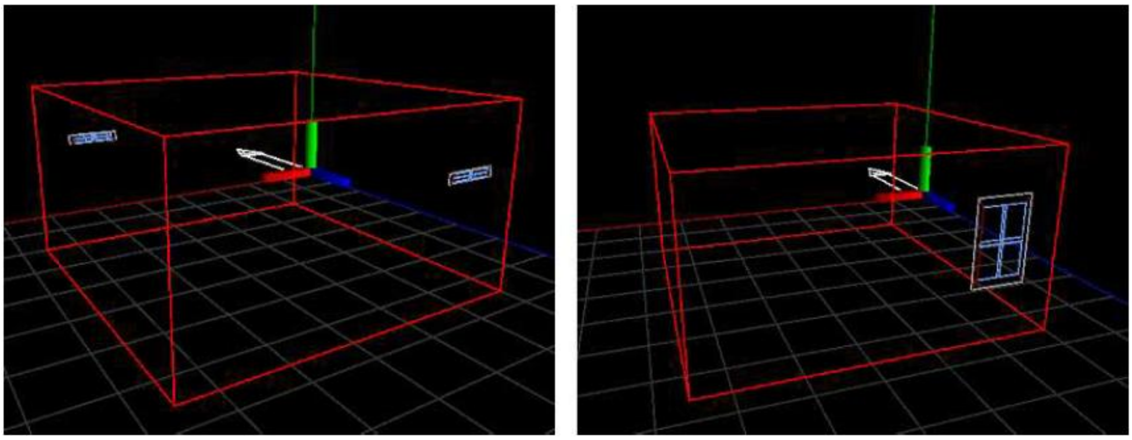

Figure 1-12: Experiments designs performed in DOMUS for the wind tunnel: (a) cross ventilation case and (b) single-sided ventilation case.

### 1.7.3 Ouputs

The following outputs are required for comparison with the experimental results:

1. Air change rates for Cross Ventilation: all available angles, wind velocity equals to 1, 3 and 5 m/s, and
2. Air change rates for Single-sided Ventilation: all available angles, wind velocity equals to 1, 3 and 5 m/s.

## 1.8 NATVENT 2 – On-Site Experiment

The following description is based on the original document written by R.Z. Freire (2010).

### 1.8.1 Introduction

The goal of this section is to validate and compare the ventilation models implemented into DOMUS by comparing the airflow rate estimation of the single-sided ventilation models of de Gids and Phaff (1982) and Larsen (Larsen and Heiselberg, 2008) to results obtained from one on-site experiment (Dascalaki *et al.*, 1999). Two methodologies for evaluating the wind pressure coefficient (Cp) have also been analyzed here considering that the pressure coefficient value is necessary as an input parameter for both cross and single-sided ventilation models: the CPCALC+ algorithm (see previous section) and the use of a surface-averaged Cp value defined by Swami and Chandra (1988).

### 1.8.2 Description

The building selected for the on-site experiment is the Institute of Meteorology and Physics of the Atmospheric Environment, which is a three-storey, naturally ventilated, office building referred as the NOA (National Observatory of Athens) building in the sequence. Each floor is about 4.50 m high and the dimensions are 10.20 m × 16.30 m of length and width respectively. Ventilation experiments were held at the first floor (IEA, 1996).

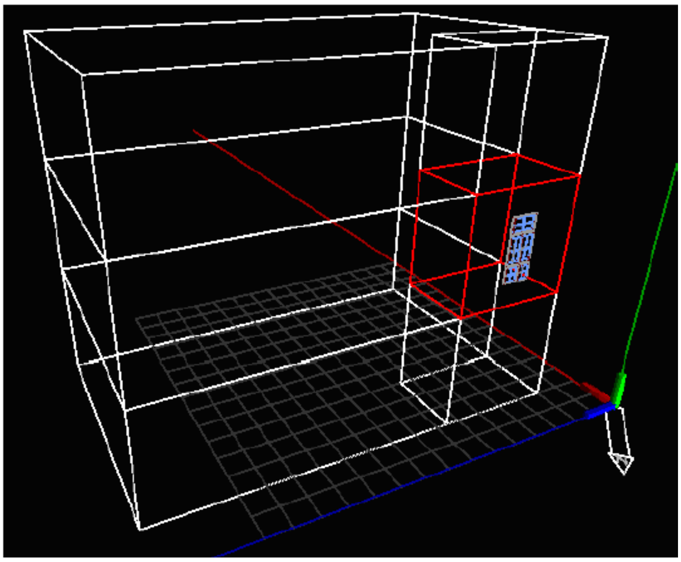

Figure 1-13: Experiment design performed in DOMUS for the on-site single-sided ventilation case.

The selected office room (Figure 1-13) was isolated from the rest of the building. The room has a 13.59 m$^2$ floor area, while its length is equal to 3.00 m. The only external window, which is shown in Figure 1-14 (Dascalaki *et al.*, 1999), is located on the west wall and is divided into five parts; each part can be opened separately providing the different opening configurations. The dimensions of each part of the opening are presented in Table 1-11, the total window area is 2.50 m$^2$ and its angle from the North orientation is 315°. Airflow rates across the openings have been performed according to the single tracer gas decay technique. Fourteen different experiments have been taken into account. The mean climatic conditions for each experiment are given in Table 1-12.

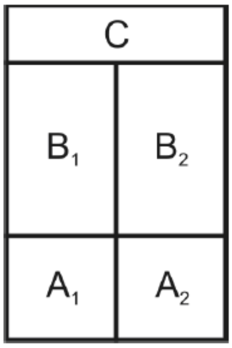


Figure 1-14: Window parts for the on-site experiment.

Table 1-11: Window dimensions for the on-site experiment.

| Window Part | Height (m) | Width (m) | Opening Area (m2) |
|---|---|---|---|
| $A_1$, $A_2$ | 0.65 | 0.53 | 0.34 |
| $B_1$, $B_2$ | 1.13 | 1.13 | 0.60 |
| C | 0.62 | 1.06 | 0.66 |

Table 1-12: Opening configurations and mean climatic conditions for single-sided ventilation experiments in the NOA building.

| Configuration | $T_i$ (°C) | $T_O$ (°C) | $U_{10}$ (m/s) | $\beta$ |
|---|---|---|---|---|
| $A_1 + A_2$ | 31.4 | 31.3 | 6.8 | 40 |
| $B_1 + B_2$ | 31.8 | 32.6 | 3.0 | 70 |
| C | 32.1 | 30.6 | 5.0 | 30 |
| $A_2 + B_2$ | 31.8 | 32.5 | 6.7 | 50 |
| $A_1 + A_2 + B_1 + B_2$ | 31.5 | 30.5 | 1.7 | 50 |
| $B_1 + B_2 + C$ | 29.2 | 28.8 | 1.6 | 45 |
| All | 31.0 | 30.2 | 3.6 | 12 |
| $A_2 + C$ | 31.7 | 31.2 | 5.4 | 30 |
| $B_2 + C$ | 31.8 | 30.7 | 4.9 | 70 |
| $A_1 + A_2 + C$ | 31.0 | 30.8 | 4.2 | 50 |
| $A_1 + B_1 + C$ | 28.8 | 27.6 | 2.0 | 35 |
| $A_2 + B_2 + C$ | 31.6 | 30.1 | 5.0 | 20 |
| $A_1 + A_2 + B_1 + C$ | 31.0 | 29.6 | 3.1 | 35 |
| $A_1 + A_2 + B_2 + C$ | 31.0 | 28.2 | 3.4 | 37 |

$T_i$ is the indoor temperature, $T_o$ is the outdoor temperature, $U_{10}$ is the wind speed at 10 m high and $\beta$ is the wind incidence angle.

### 1.8.3 Ouputs

The outputs that are required for comparison with the experimental results are the air change rates for all window configurations.

# 2 RESULTS AND DISCUSSION

## 2.1 HAMSTAD – Analytical Benchmark n°2

All material properties are constant with the exception of the sorption isotherm which is a function of the relative humidity. DOMUS uses tabulated data to take the sorption effect into consideration. A total of 100 pairs of moisture content (in $m^3/m^3$) – relative humidity has been used for the present analysis (Figure 2-1). 200 finite volumes have been used for the spatial discretization of the slab (finite volume length of 1mm).

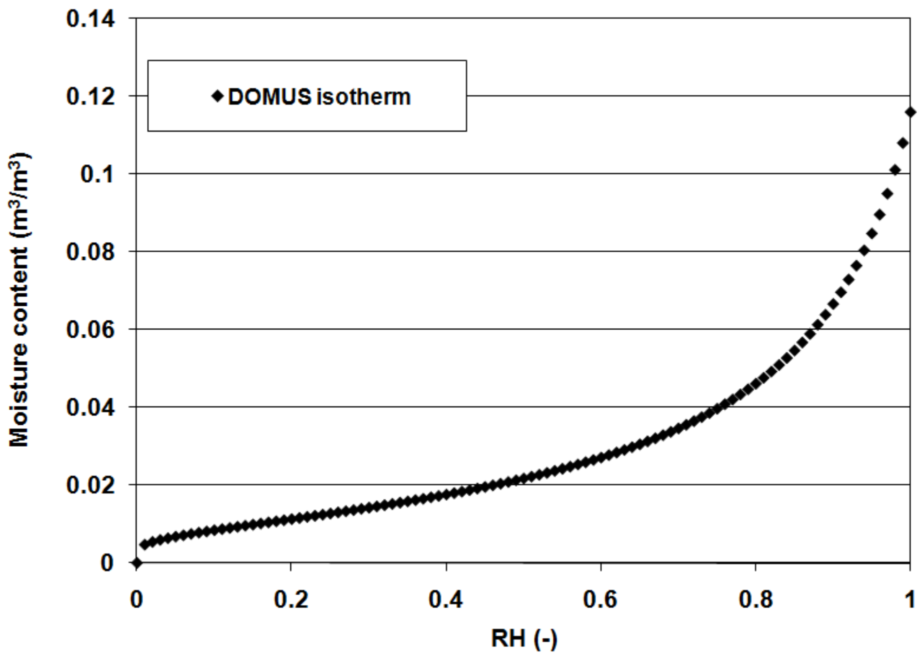


Figure 2-1: Sorption isotherm – DOMUS.

### 2.1.1 DOMUS Results

Figure 2-2 presents the moisture content distribution for the three times obtained with DOMUS. Three different time steps have been tested. As observed in the figure, the results are not dependent on the time step value for time step lower than 2 minutes.

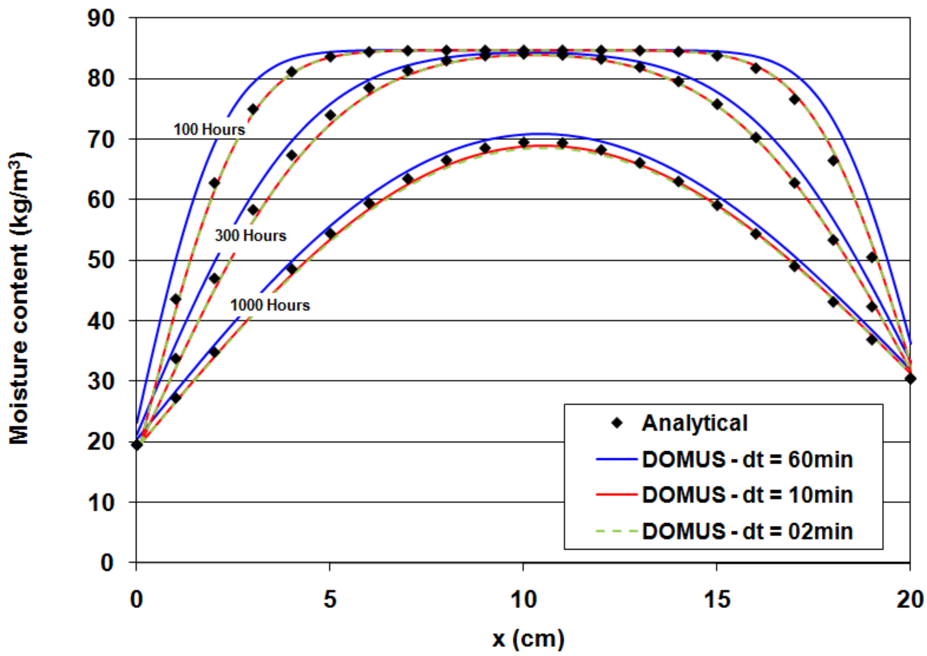


Figure 2-2: Moisture content distribution for time 100, 300 and 1000 hours – DOMUS results.

### 2.1.2 Comparison with other simulation programs

The correlation coefficients with the analytical solution are presented for all simulation programs that have participated to the original benchmark and DOMUS for the three times (Figure 2-3 to Figure 2-5).

The participants of the original benchmark were University of Leuven (KUL), Chalmers University of Technology (CTH), Technical University of Dresden (TUD), Technion Israel Institute of Technology (Technion), TNO Building and Construction Research (TNO) and National Research Council of Canada (NRC).

DOMUS performs as well as the other programs, however some slightly higher errors are observed for times 300 and 1000 hours. Those differences can come from rounded materials properties and convection coefficients at the material surface imposed by DOMUS graphical interface.

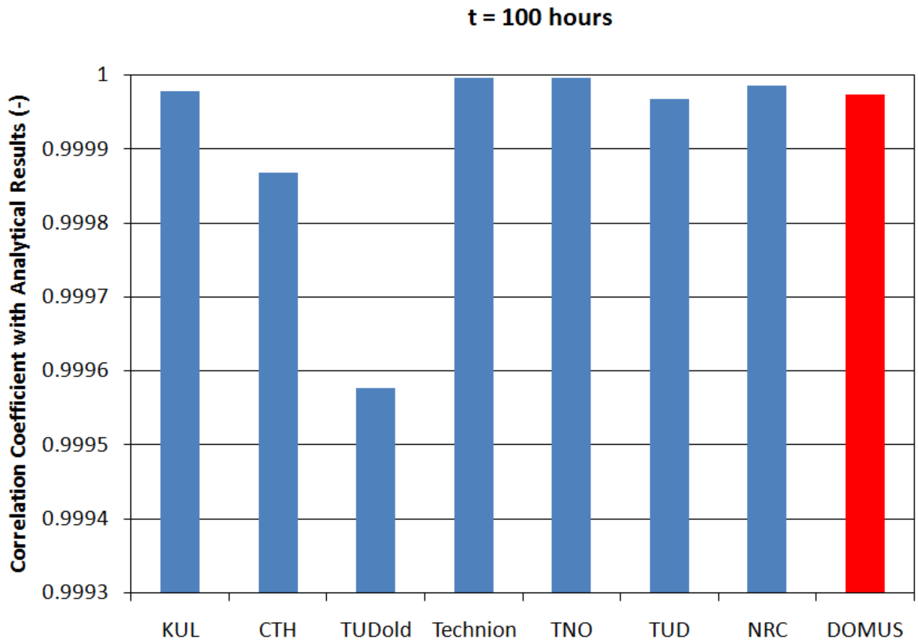


Figure 2-3: Correlation coefficient with Analytical Solution – t = 100 hours.

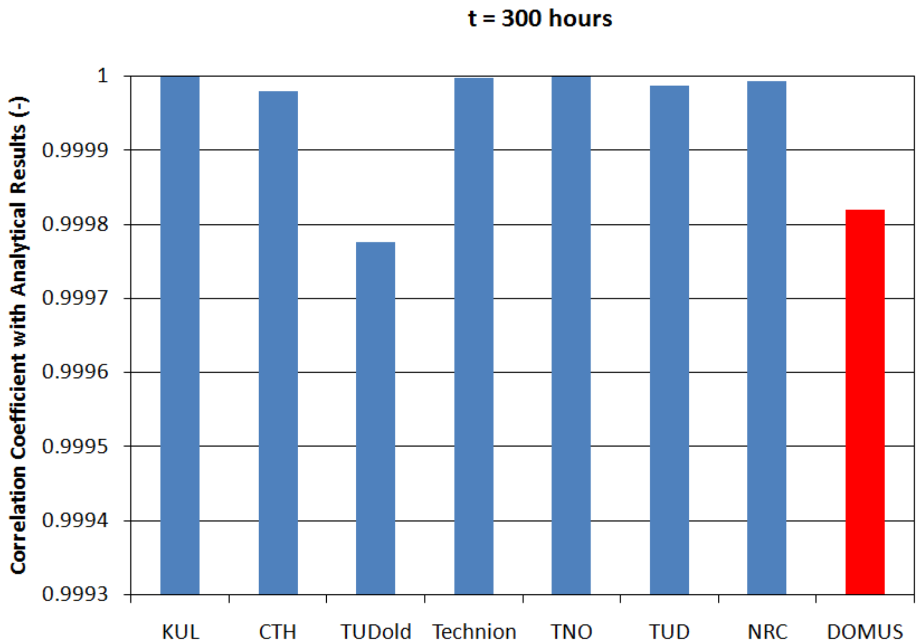


Figure 2-4: Correlation coefficient with Analytical Solution – t = 300 hours.

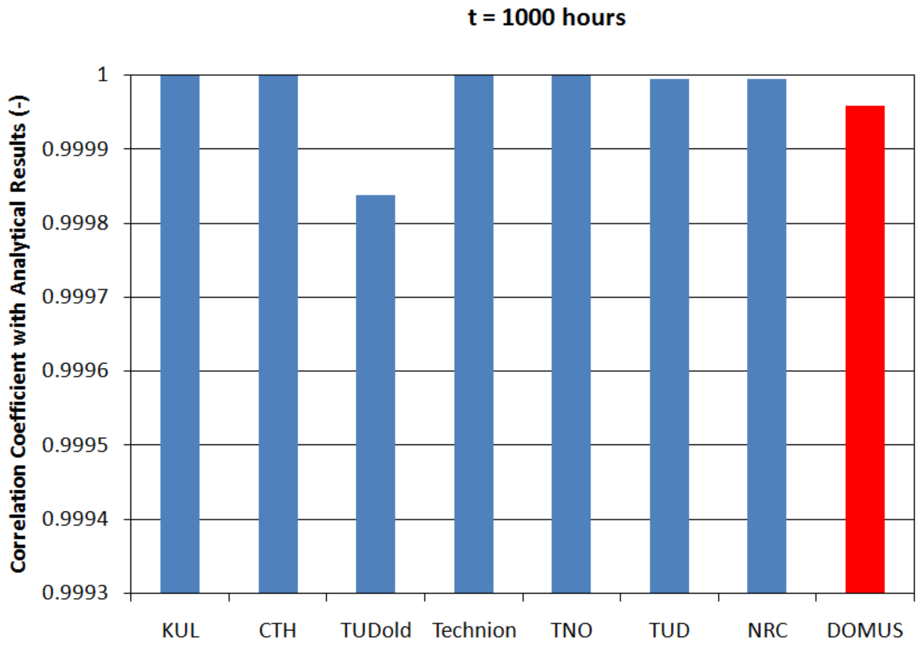


Figure 2-5: Correlation coefficient with Analytical Solution – t = 1000 hours.

### 2.1.3 Conclusion

For the present benchmark, DOMUS gives results as good as the other simulation programs. Note that rounded materials properties and convection coefficients at the material surface imposed by DOMUS graphical interface, and not by the program itself, can explain the existence of some results that are slightly farther from the analytical solution.

## 2.2 ANNEX 41 Subtask 1 – Common Exercise 1A and 1B

The main focus here is the evolution of the relative humidity with time. Material properties have been converted to DOMUS inputs. Regarding the discretization of the wall material layers, each finite volume has a maximal dimension of 1cm. A time step of 1 minute has been used for all simulations.

### 2.2.1 DOMUS Results for Exercise 1A

The purpose of this example is to calculate the relative humidity of the zone air with impermeable wall internal surfaces to verify that DOMUS correctly calculate the vapor mass conservation. Figure 2-6 presents the evolution of the zone air relative humidity when there is no moisture transfer to the walls. DOMUS perfectly matches the analytical solution.

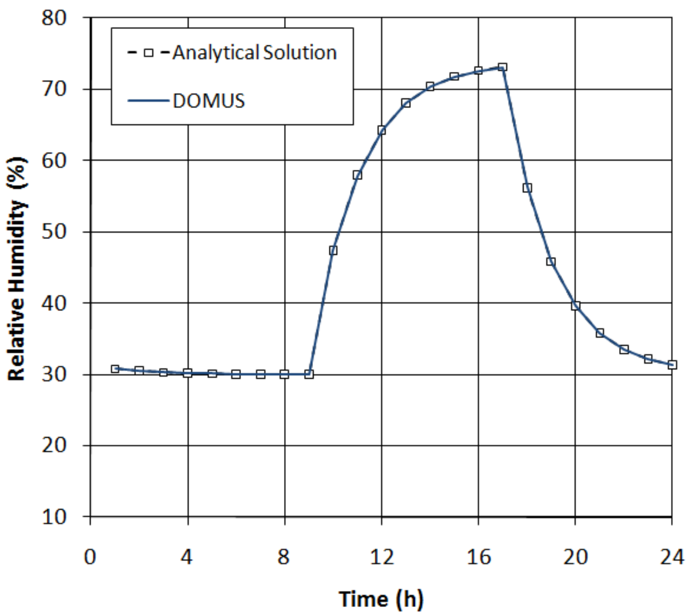


Figure 2-6: Relative Humidity versus time – Case 1A.

### 2.2.2 DOMUS Results for Exercise 1B

Figure 2-7 and Figure 2-8 present the relative humidity evolution within the zone taking the wall buffer storage into account for the three first days and when the periodic state is achieved. The periodic state is reached when the relative difference between two consecutive days relative humidity is lower than 0.01 % for each hour of the 24 hour period. Results clearly show that DOMUS gives accurate predictions for the present problem with a maximal difference of 0.3%RH.

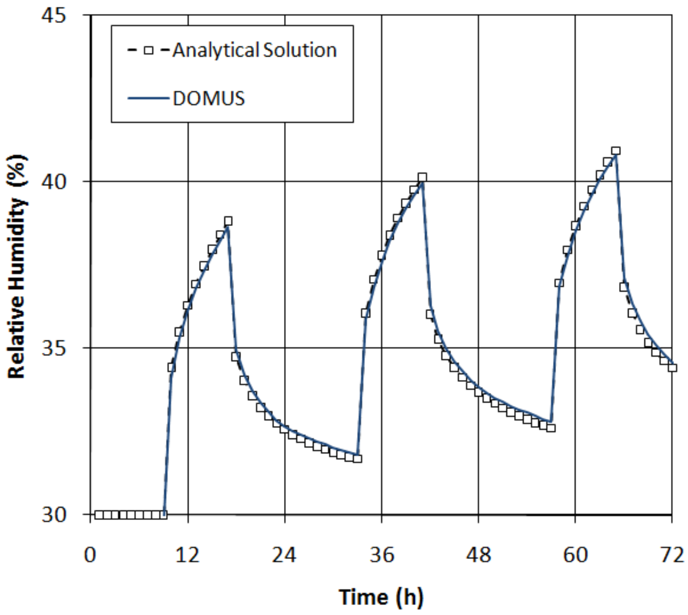


Figure 2-7: Relative Humidity versus time for the three first days – Case 1B.

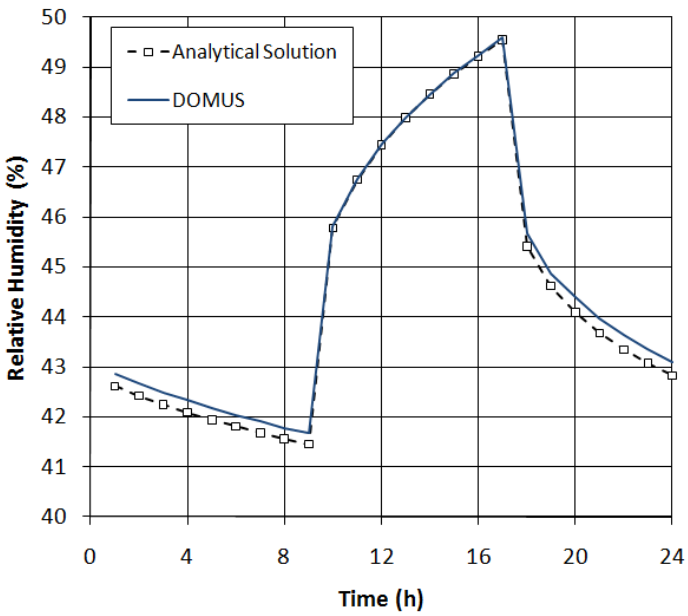


Figure 2-8: Relative Humidity versus time when periodic state is reached – Case 1B.

### 2.2.3 Conclusion

The present validation aimed at testing the capabilities of DOMUS to model the relative humidity variation of a room air when subjected to a periodic vapor release considering or not the presence of the envelop porous materials under isothermal conditions. DOMUS successfully predicts the variations of the room air relative humidity.

## 2.3 ANNEX 41 Subtask 1 – Common Exercise 3 (Whole building heat and moisture analysis)

In the following the results of the calculations of DOMUS validation are shown for few days of the period of measurements (step 1, 2 and 3). The main focus here is the evolution of the relative humidity with time. Material properties have been converted to DOMUS inputs. Regarding the discretization of the wall material layers, each finite volume has a maximal dimension of 1cm. A time step of 1 minute has been used for all simulations.

### 2.3.1 DOMUS Results

Figure 2-9 to Figure 2-12 present the evolution of the relative humidity and heating power for both the reference and test rooms for two exemplary days of the Step 1 period of measurements. This test shows the differences between the reference room and the test room with aluminium foil. DOMUS correctly represents the relative humidity variation in the test room (Figure 2-10) where no sorption effects were possible. However, DOMUS tends to overestimate the moisture buffer effect of the painted gypsum boards present in the reference room (Figure 2-9) where the relative humidity amplitude is slightly underpredicted compared to the experimental one. Figure 2-11 shows a clear trend of overestimation of DOMUS regarding the heating power related to the reference room. This trend can be explained by the initial assumption of perfectly well-mixed zone employed by Building Energy Simulation programs known as single-node or nodal methodology. It is assumed that the air within the studied zone (i.e. the room) is spatially and instantaneously homogeneous in temperature and moisture. However, in reality, the source of heat is spatially localized in a limited region of the whole room volume and does not respond instantaneously to the change of temperature. As a result, the real heat source will tend to consume more energy than the heating energy calculated by the nodal approach. Figure 2-12 presents the heating power evolution for the test room. Unfortunately, as observed around the 26/01/2005, the sensor of the test room broke during the experiment. As a result, the heating power will be shown only for the reference rooms for the next steps.

Figure 2-13 to Figure 2-15 present the results for Step 2. In this case, unpainted gypsum boards have been attached on top of the walls (50 m²) of the test room. Underestimation of the moisture buffer effect is observed in the test room contrary to it was measured in the reference room during Step 1. However, the same underestimation is observed for the heating power variation.

Figure 2-16 to Figure 2-18 present the comparisons for Step 3. A total of 65 m² of unpainted gypsum boards is now present in the test room. This time, DOMUS correctly represents the evolution of relative humidity in the test room. Same trend is observed for the heating power variation than in Step 1 and 2.

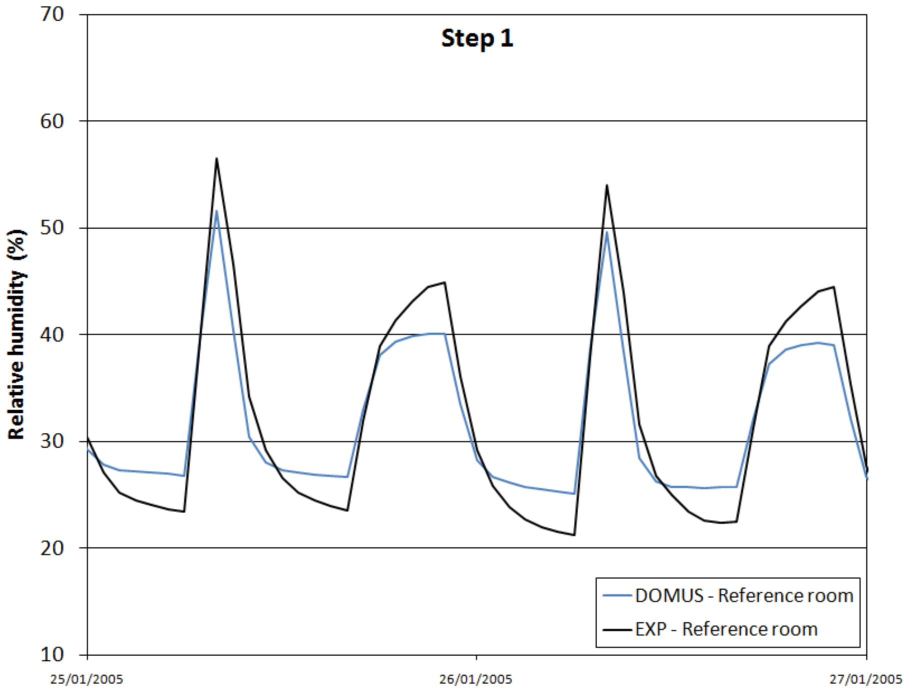


Figure 2-9: Relative humidity variation with time – Reference Room – Step 1.

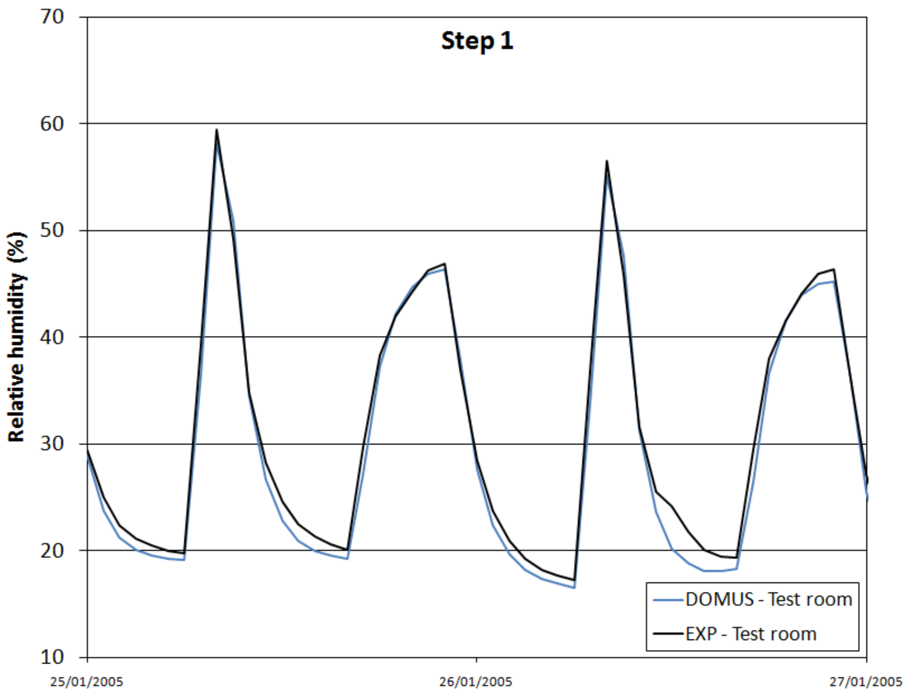


Figure 2-10: Relative humidity variation with time – Test Room – Step 1.

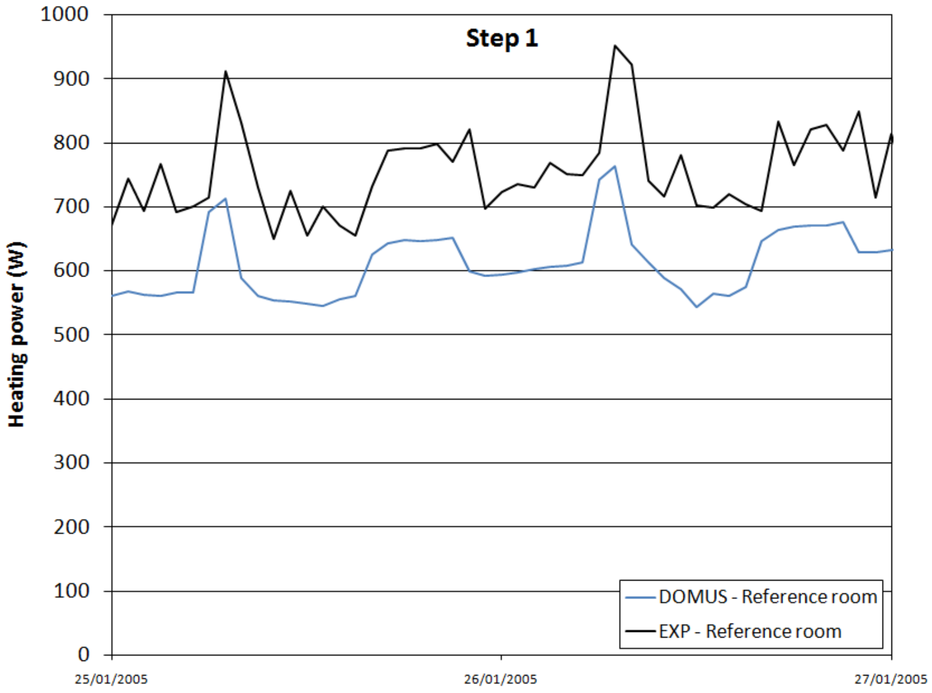


Figure 2-11: Heating energy variation with time – Reference Room – Step 1.

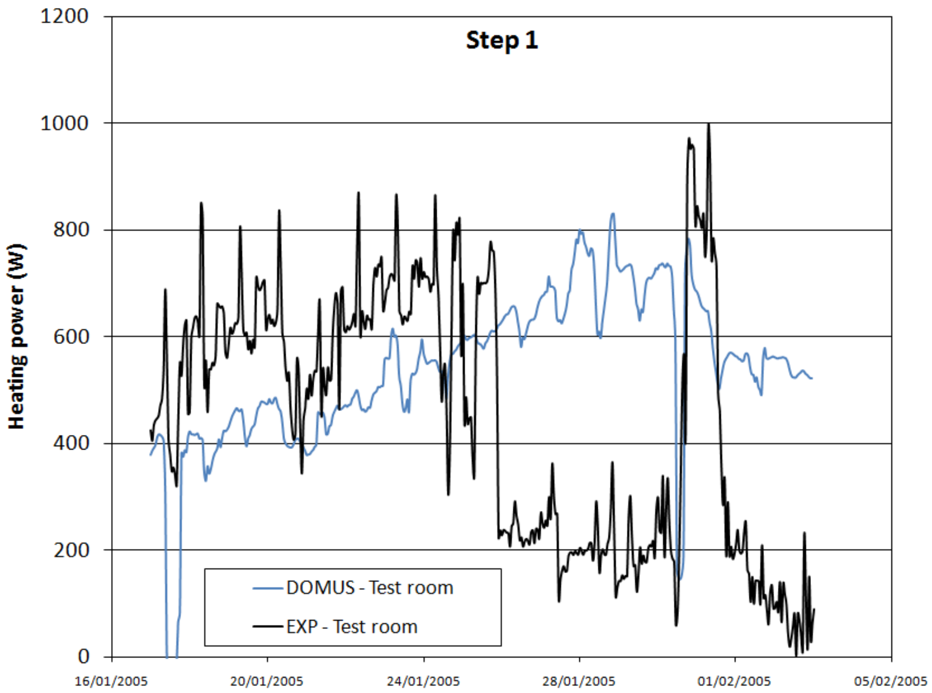


Figure 2-12: Heating energy variation with time – Test Room – Step 1.

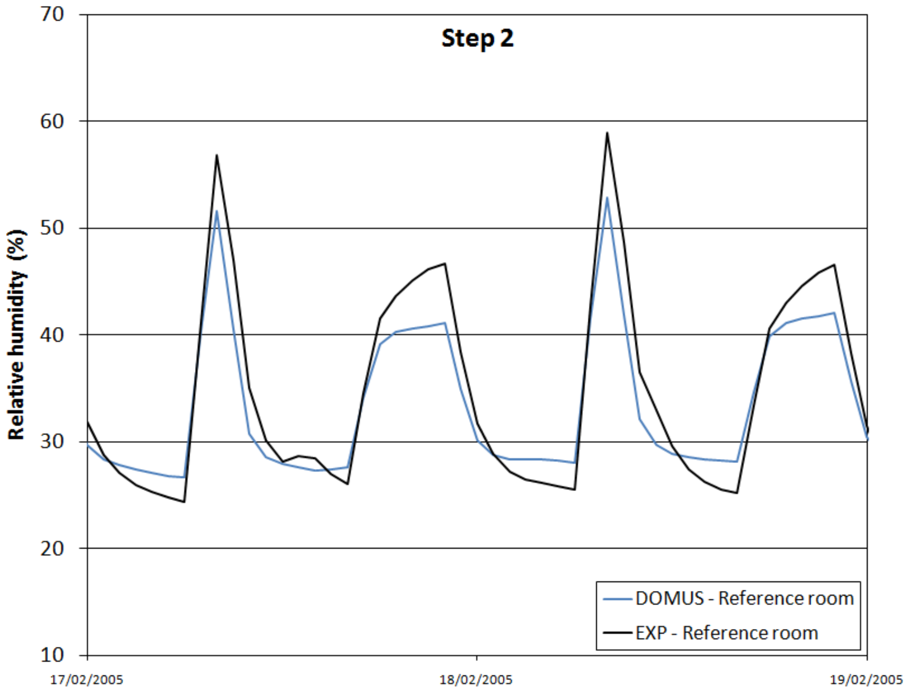


Figure 2-13: Relative humidity variation with time – Reference Room – Step 2.

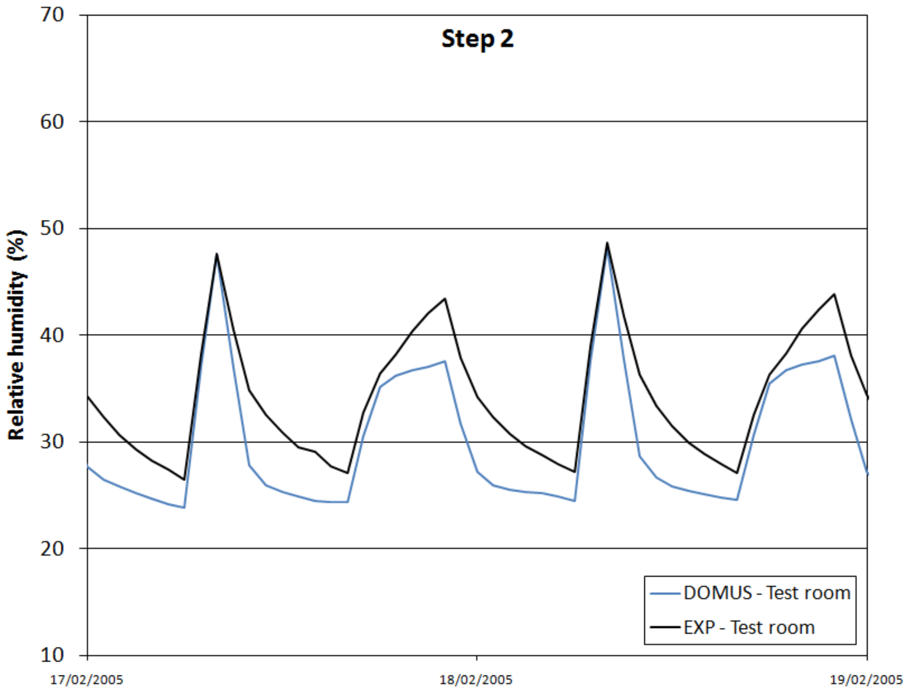


Figure 2-14: Relative humidity variation with time – Test Room – Step 2.

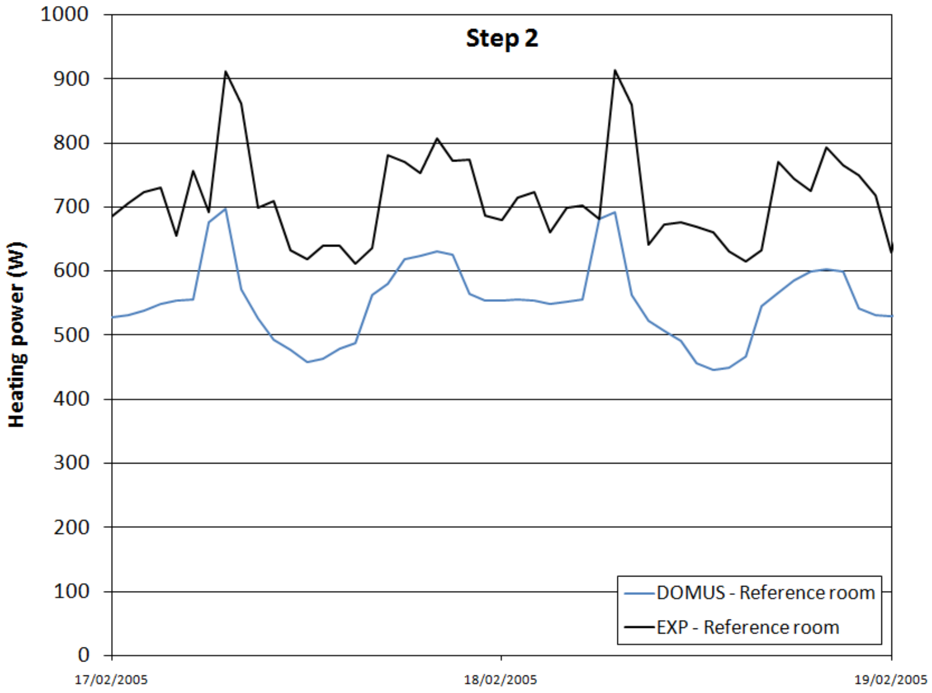


Figure 2-15: Heating energy variation with time – Reference Room – Step 2.

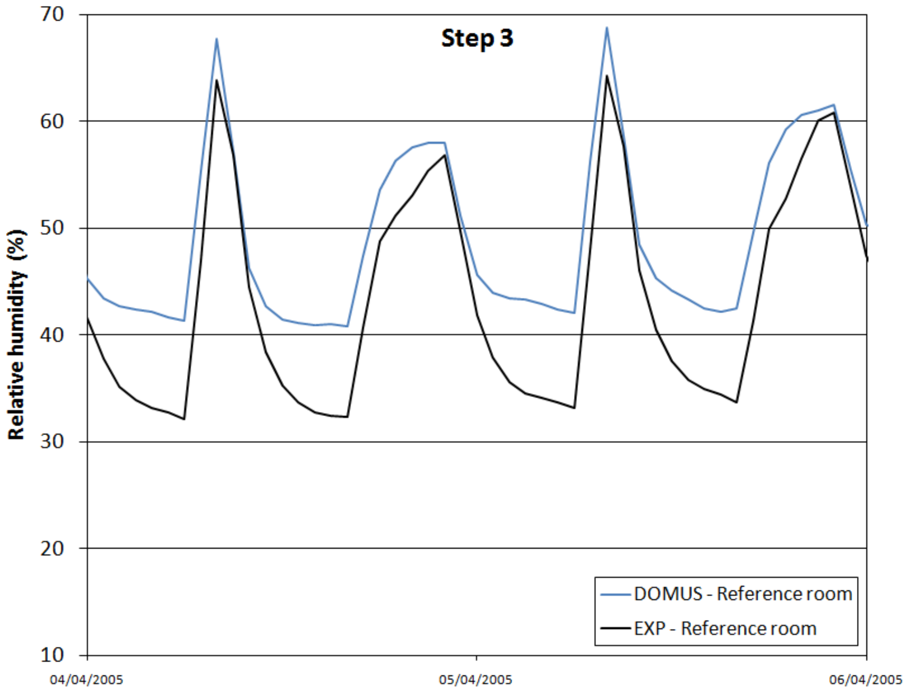


Figure 2-16: Relative humidity variation with time – Reference Room – Step 3.

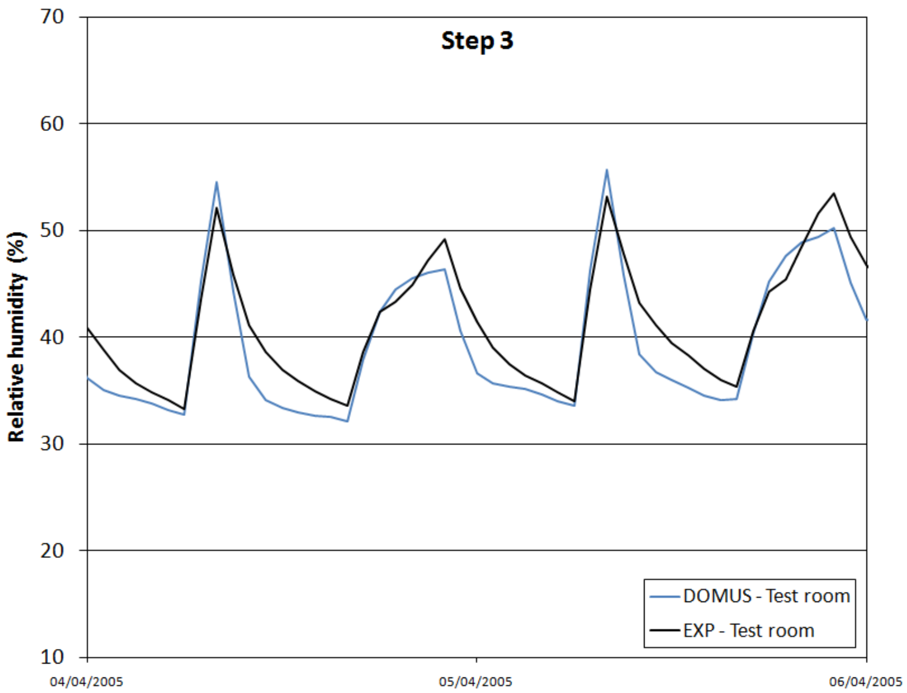


Figure 2-17: Relative humidity variation with time – Test Room – Step 3.

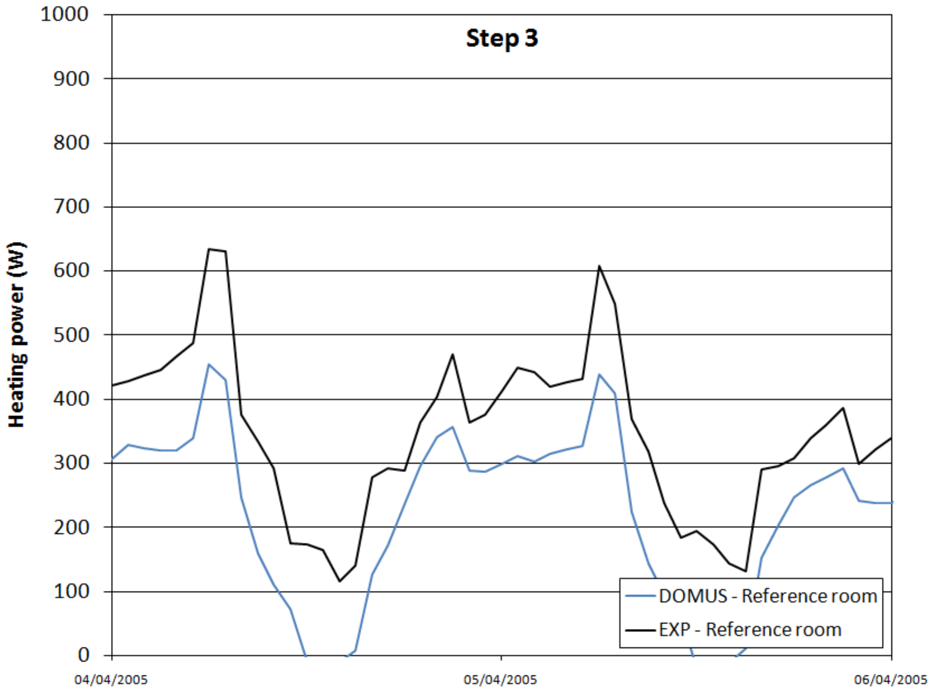


Figure 2-18: Heating energy variation with time – Reference Room – Step 3.

### 2.3.2 Comparison with other simulation programs

Table 2-1 presents the participants of the original benchmark. In the following figures, TESTroom and REFroom are used to present the measurement results, the simulation tools are noted Model i (i from 1 to 13). DOMUS is Model7, highlighted with the blue color in the figures. For each period of measurements, mean, median, 25-75% percentile, maximal and minimal values of relative humidity and heating power have been calculated for the test and reference rooms.

Table 2-1: Participating institutions and simulation tools used for the benchmark.

| Institutions | Country | Simulation tools |
|---|---|---|
| CETHIL | France | Clim2000 |
| CON | Canada | HAMFitPlus (COMSOL + MatLab + Simulink) |
| CTH | Sweden | HAM-Tools |
| DTU | Denmark | BSim, Version 4,5,6,7 |
| FhG | Germany | Raummodell 1.0 pro<br>WUFI®-Plus Version 1.0.1.24 |
| PUCPR | Brazil | DOMUS<br>TRNSYS 15.3 |
| SAS | Slovakia | ESP-r, NPI |
| TUD | Germany | TRNSYS-ITT |
| TUE | Netherlands | HAMLab |
| TTU | Estonia | IDA Indoor Climate and Energy (IDA ICE) Version: 3.0 Build 14 |
| TUW | Austria | BUILTOPT-VIE |
| UG | Belgium | TRNSYS 16.00.0036 |

Figure 2-19 to Figure 2-21 show the results of the statistical analyses for Step 1 in the test room with aluminium foil and in the reference room with painted gypsum plaster. For the test room, the variations of the medians and percentiles of Step 1 show good agreements of the different models to the measurement. Results for the reference room are a bit more dispersed. The statistical analysis of the heating power in the reference room presents a very high spreading of the results.

The same statistical analyses were done for Step 2, the test room with 50 $m^2$ of unpainted gypsum boards on the walls and the reference room with painted gypsum plaster on the walls and the ceiling. The results are presented in Figure 2-22 to Figure 2-24. In this case the variation between the simulations and the measurement are partly higher for relative humidity. Most models have considerable trouble at calculating the heating power in the room correctly.

Figure 2-25 to Figure 2-27 present the results for Step 3 with 65 $m^2$ of unpainted gypsum boards on the walls and the ceiling in the test room. The results of the descriptive statistic show similar results as for Step 2 for both relative humidity and heating power.

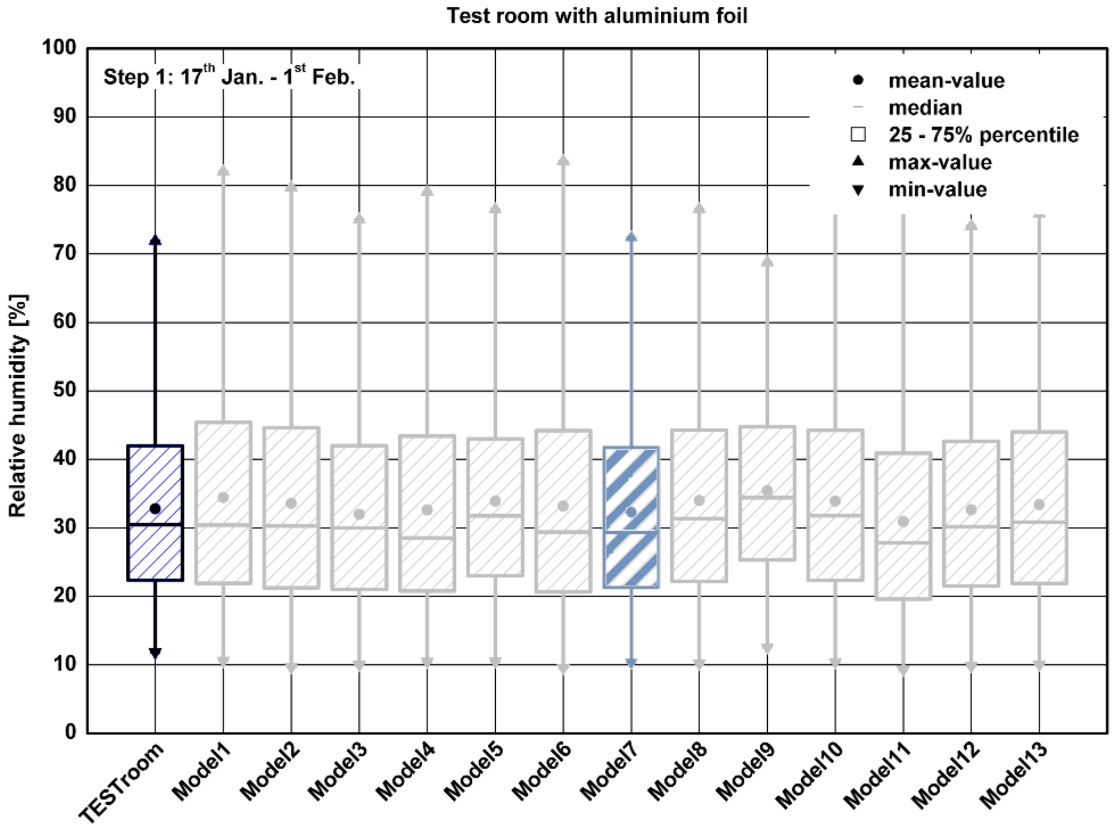


Figure 2-19: Comparative analysis of the Relative Humidity – Test Room – Step 1.

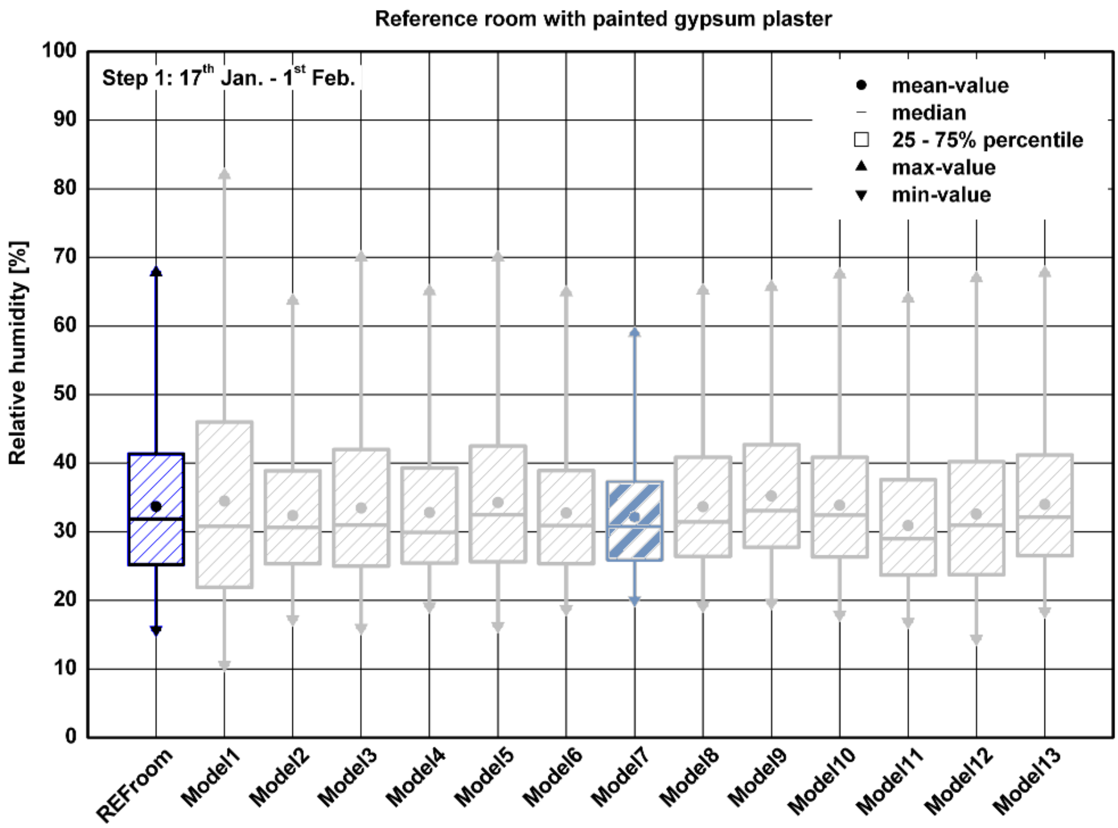


Figure 2-20: Comparative analysis of the Relative Humidity – Reference Room – Step 1.

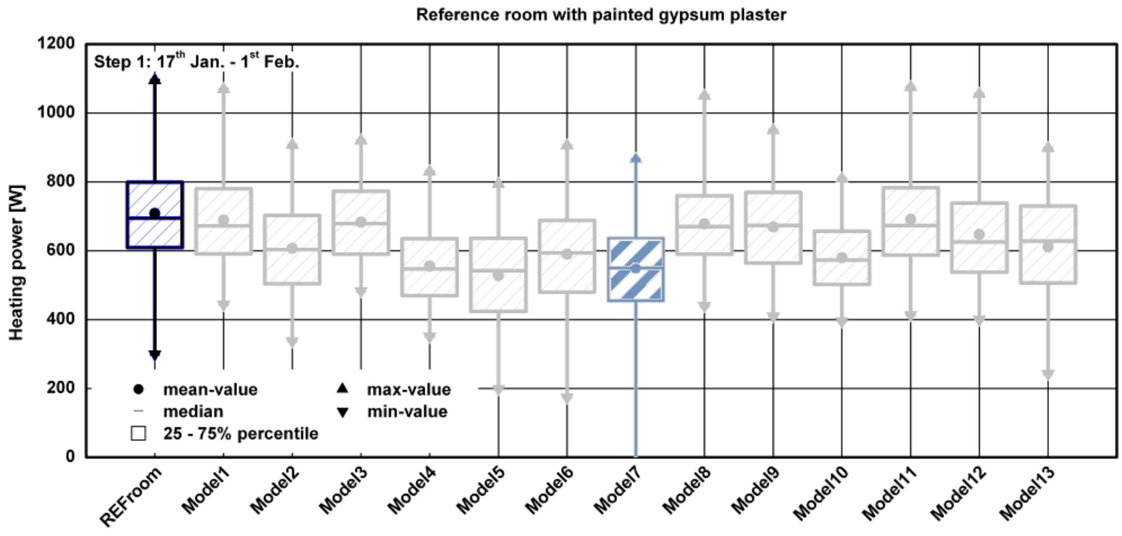


Figure 2-21: Comparative analysis of the Heating Power – Reference Room – Step 1.

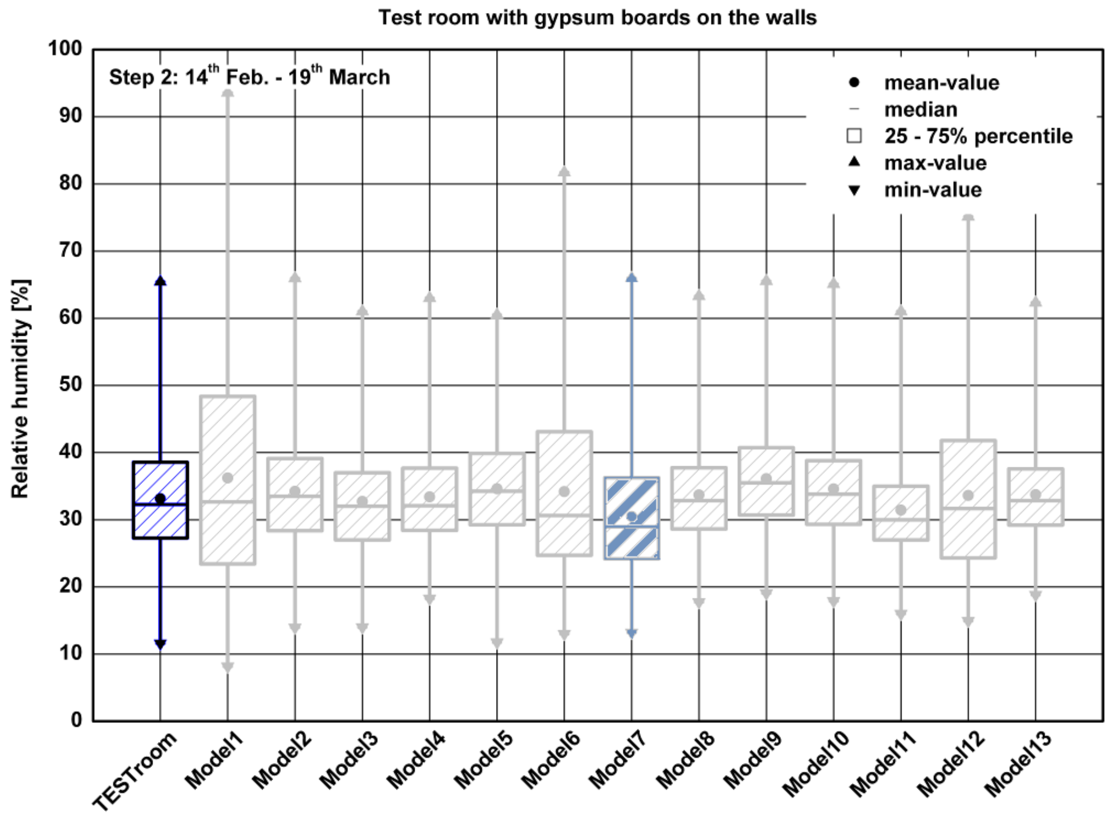


Figure 2-22: Comparative analysis of the Relative Humidity – Test Room – Step 2.

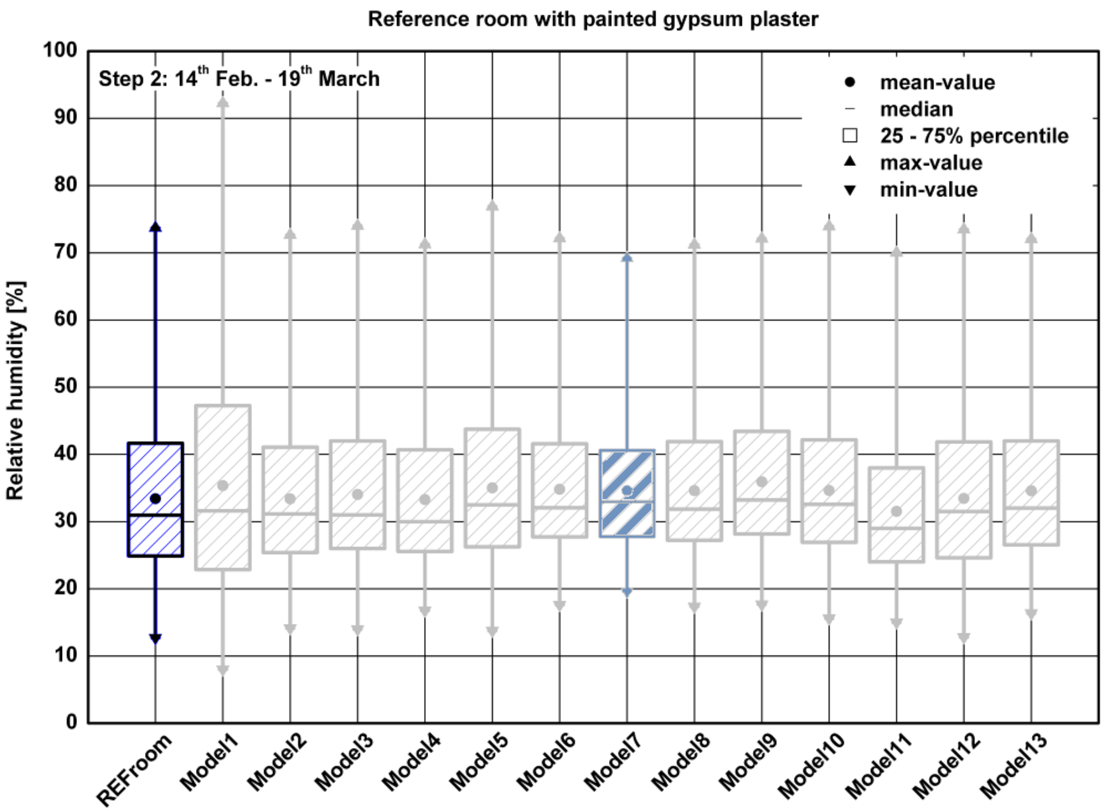


Figure 2-23: Comparative analysis of the Relative Humidity – Reference Room – Step 2.

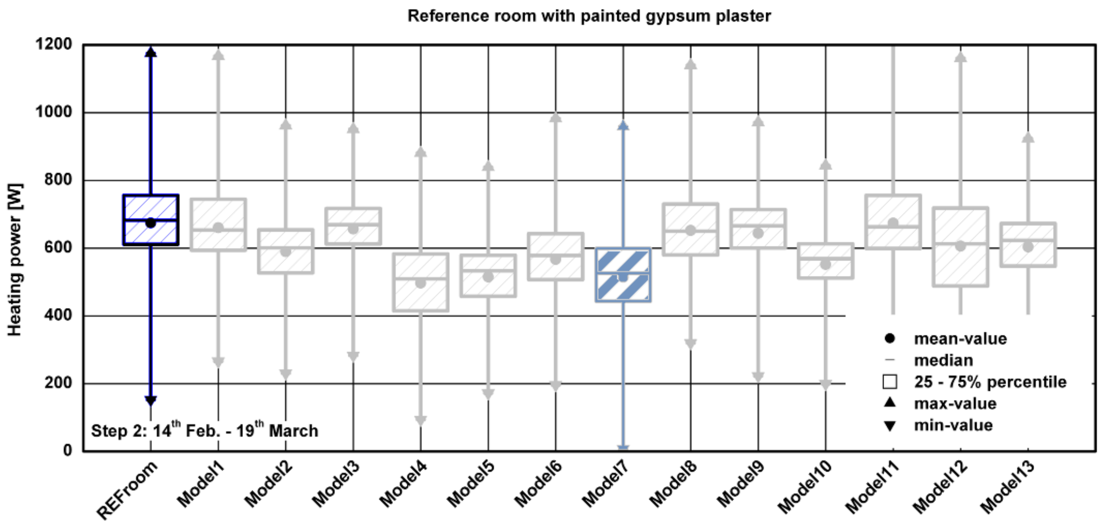


Figure 2-24: Comparative analysis of the Heating Power – Reference Room – Step 2.

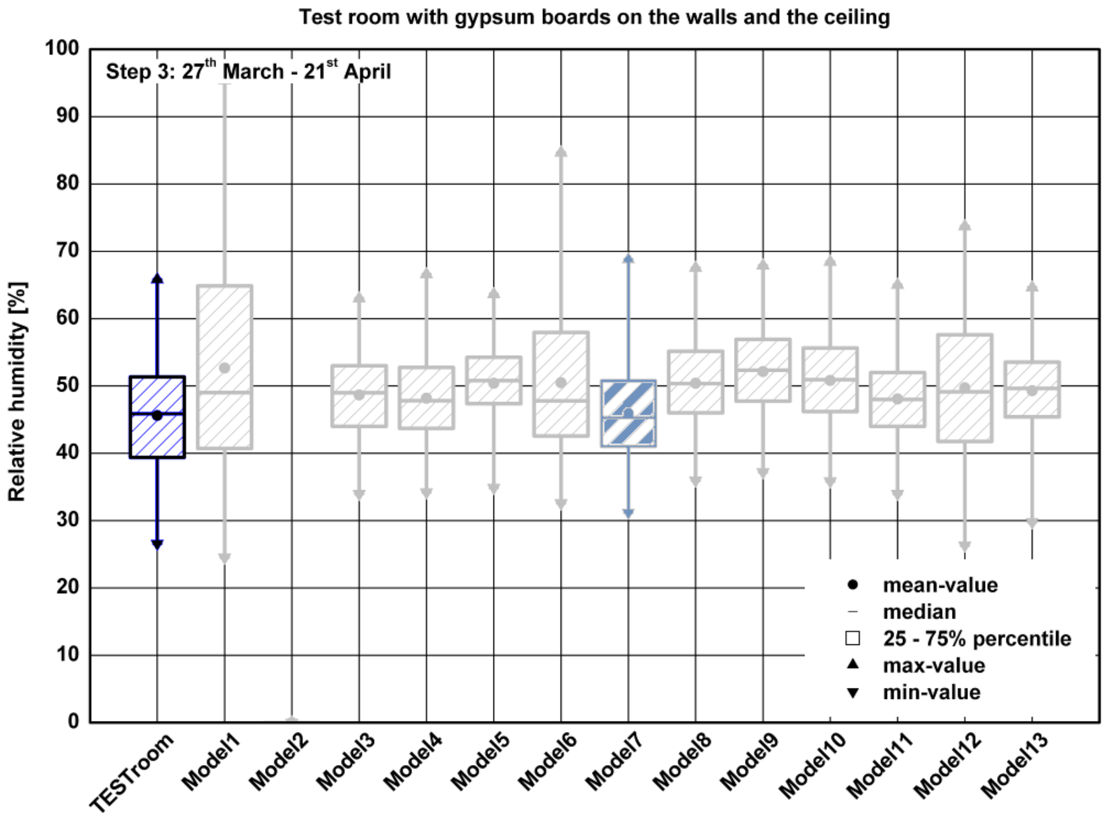


Figure 2-25: Comparative analysis of the Relative Humidity – Test Room – Step 3.

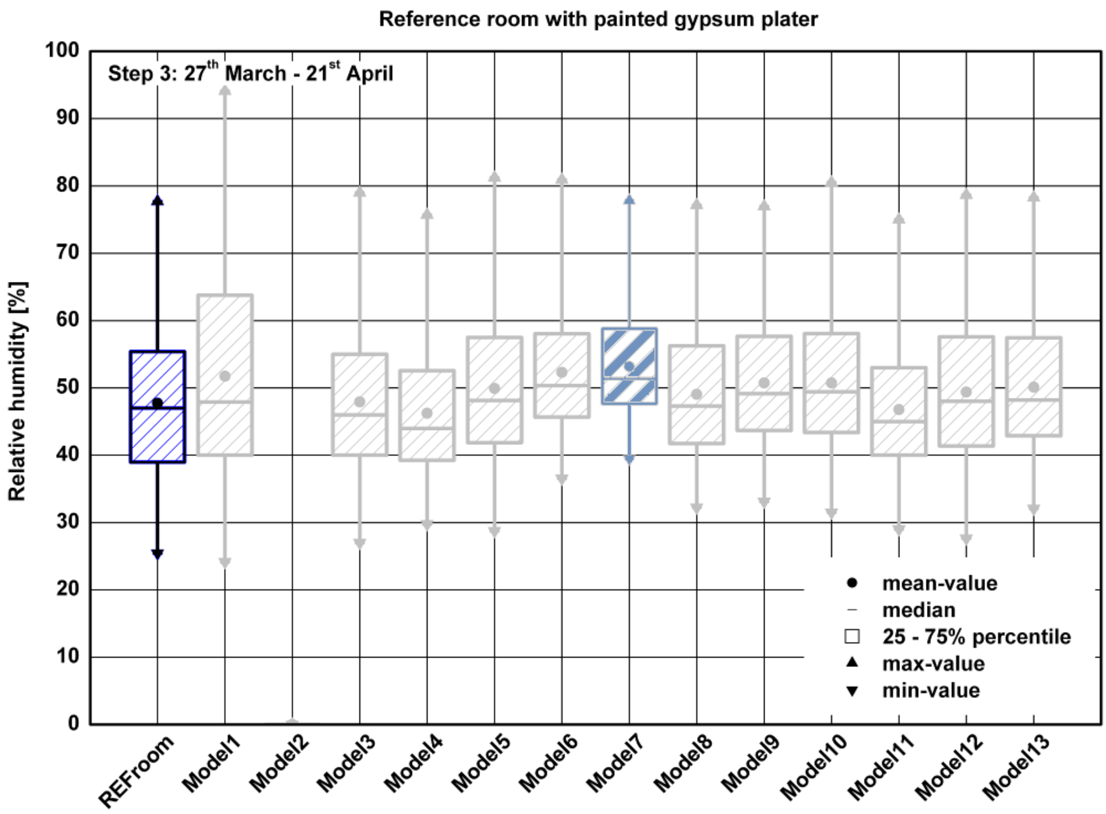


Figure 2-26: Comparative analysis of the Relative Humidity – Reference Room – Step 3.

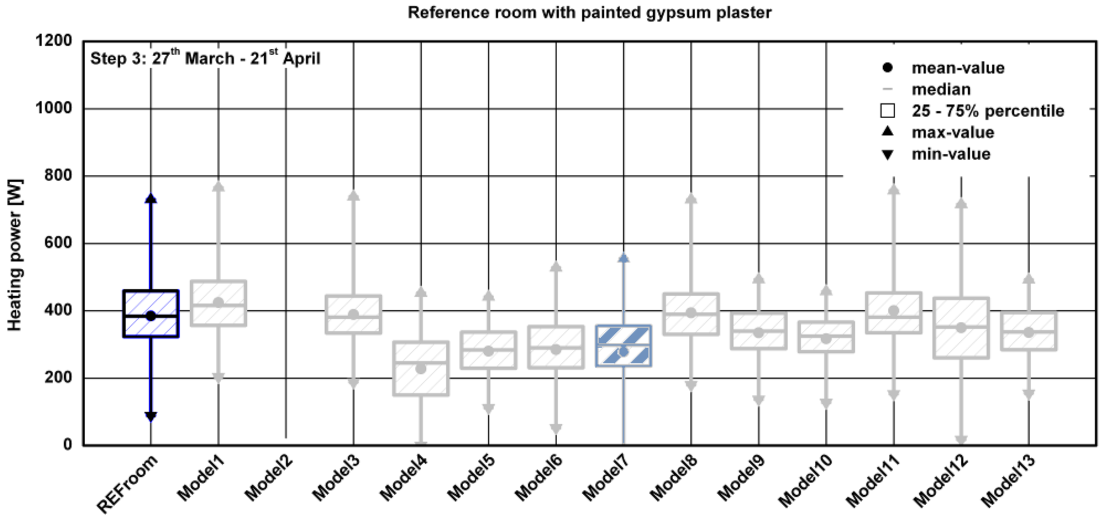


Figure 2-27: Comparative analysis of the Heating Power – Reference Room – Step 3.

### 2.3.3 Conclusion

The statistical analyses were made to point out how good are the simulation tools are and where are the problems for the calculation of the indoor climate. All the models could calculate the indoor relative humidity within a correlation of minimum 97 % inside the test room with no sorptive surfaces inside. But with gypsum boards which have a good moisture buffering behaviors, most of the models have difficulty in modeling the indoor relative humidity correctly. The results show a correlation between the measurement and the simulation close to 80 %.

DOMUS performs as well as the other simulation tools that have been used during the benchmark. Sometimes, it gives results closer to the experimental ones. In other cases, it presents larger differences with the measurements. Those differences can originate from various sources:

- The assumption of well-mixed volume can be erroneous to represent what is actually occurs in the real rooms.
- The experimental set-up can suffer problems like the broken sensor of the test room. The production of moisture can also be problematic to maintain constant during such a period of time.
- The almost always necessary conversion of the moisture-dependant properties of the porous media involves various approximations and/or simplifications.
- Abadie and Mendes (2006b) have studied the importance of the convective moisture transfer coefficient. After a systematic parametric analysis, they conclude that the discrepancies observed between the simulation and the experimental results may be originated from the value of the convective moisture transfer coefficient evaluated from the vapor diffusion thickness (sd-value). This sd-value has to be increased for both TRNSYS and DOMUS in order to fit the experimental data.

- The user of the computational tool is another source of direct and/or interpretation errors. Note that even if several institutions used the same simulation tool, they never obtained the same answer or the same trend.

## 2.4 MBV – PUCPR

### 2.4.1 Preliminary note

In order to simulate the MBV-PUCPR experiment, knowledge of the tested porous material properties are required. They include density, specific heat, porosity, sorption isotherm and coefficients of moisture (liquid and vapor) transport associated with a temperature and moisture content gradients. However, those properties for the tested wood have not been determined. Hence, the strategy employed here to reproduce the experiment has been to test three porous materials already included in the DOMUS database. The chosen materials, whose present very different properties associated to moisture, are Plaster, Brick and Wood. The dry-basis properties of the simulated materials are presented by Table 2-2. Figure 2-28 and Figure 2-29 show the sorption isotherms and variation of heat conductivity according to saturation, respectively. Figure 2-30 to Figure 2-33 present the coefficients of moisture transport associated with a temperature and moisture content gradients for total moisture (liquid+vapor) and vapor.

Table 2-2: Dry-basis properties of the simulated materials.

| | Dry-basis density ($kg/m^3$) | Specific heat (J/kg.K) | Dry-basis heat conductivity (W/m.K) | Porosity (-) |
|---|---|---|---|---|
| **Plaster** | 2050 | 932 | 0.72 | 0.18 |
| **Brick** | 1900 | 920 | 0.749 | 0.29 |
| **Wood** | 400 | 1500 | 0.09 | 0.73 |

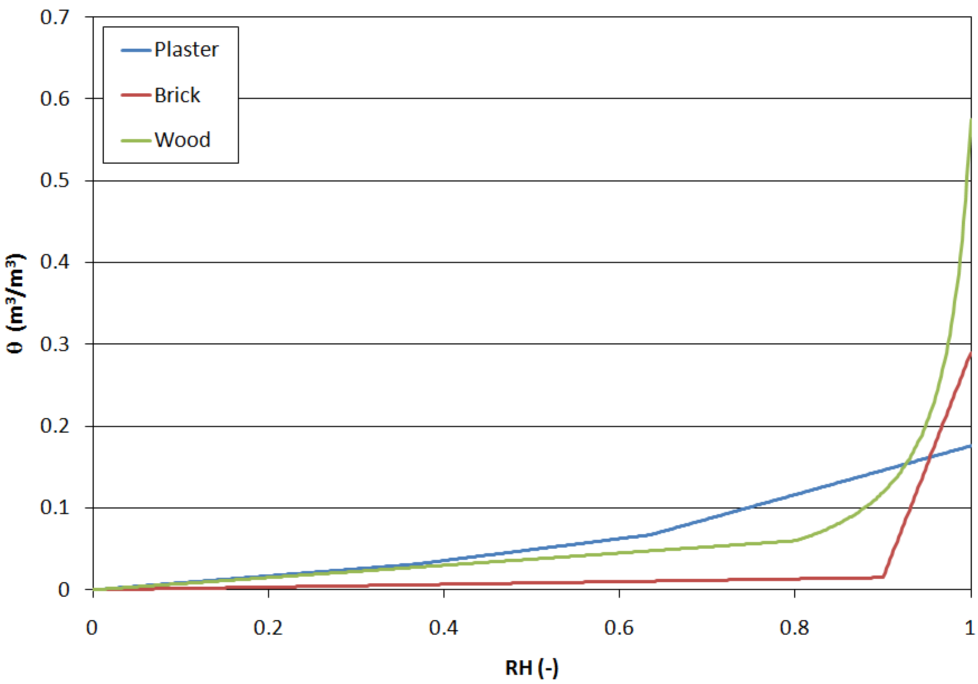


Figure 2-28: Sorption isotherm.

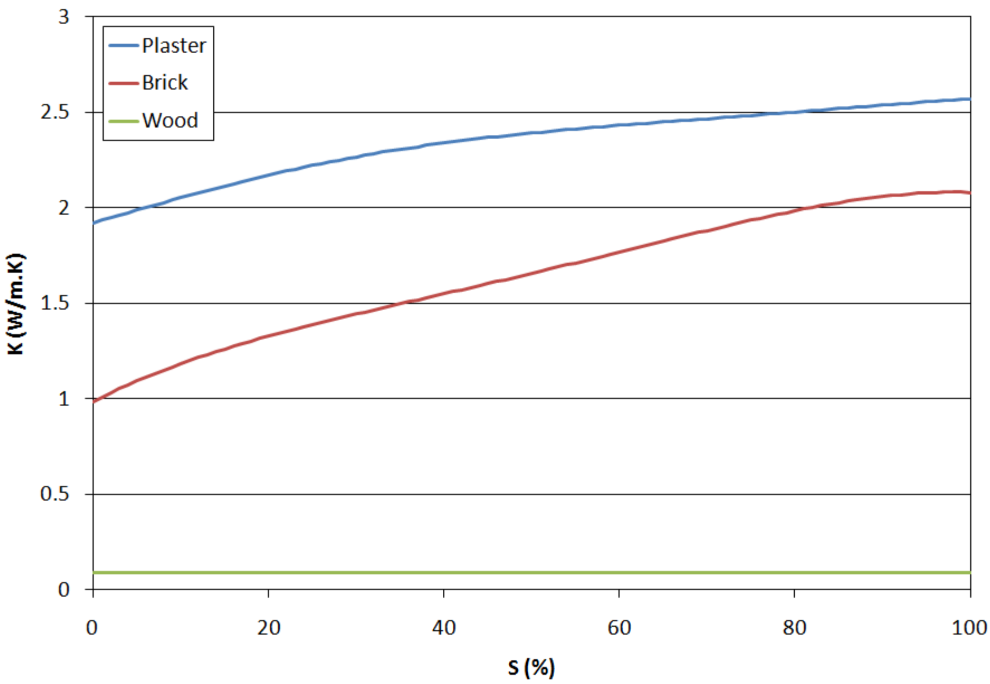


Figure 2-29: Heat conductivity versus saturation.

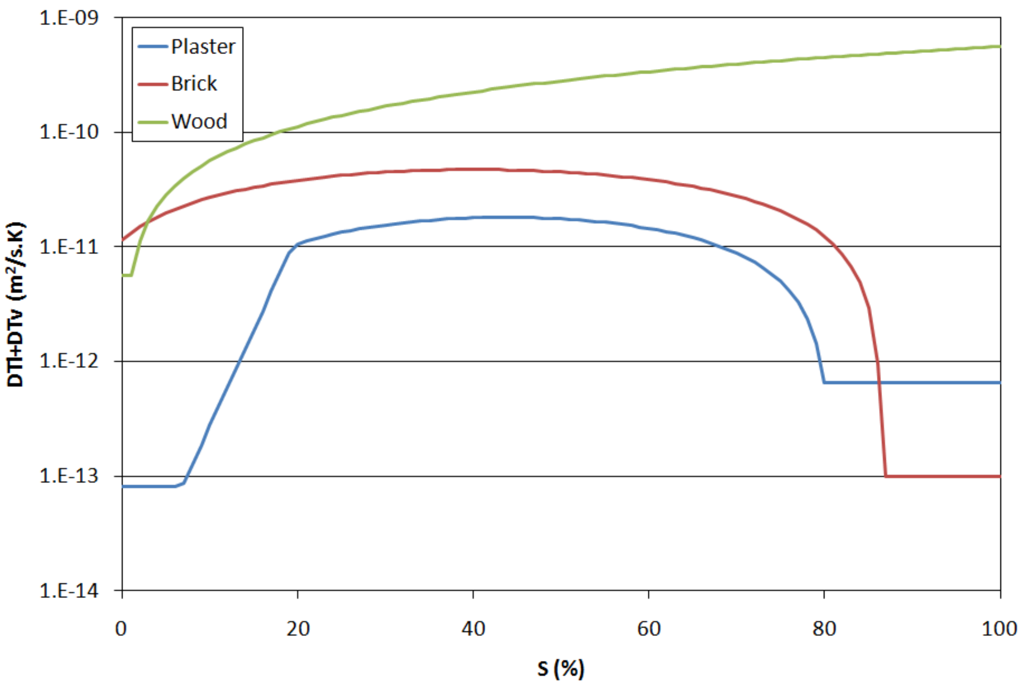


Figure 2-30: Coefficient of moisture transport associated with a temperature gradient (liquid+vapor) versus saturation.

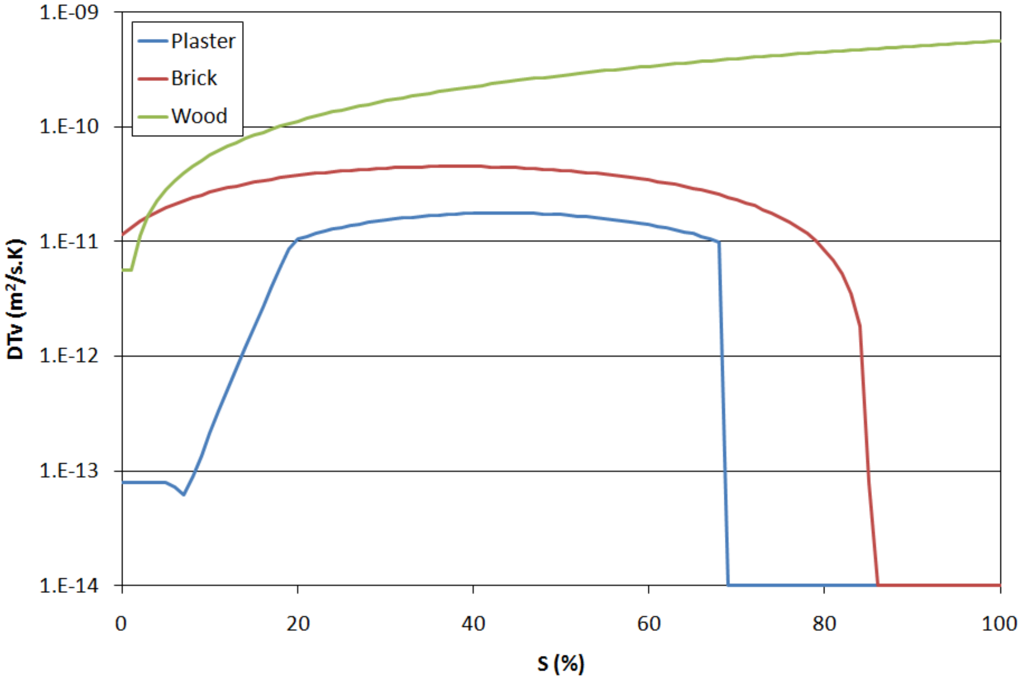


Figure 2-31: Coefficient of moisture transport associated with a temperature gradient (vapor only) versus saturation.

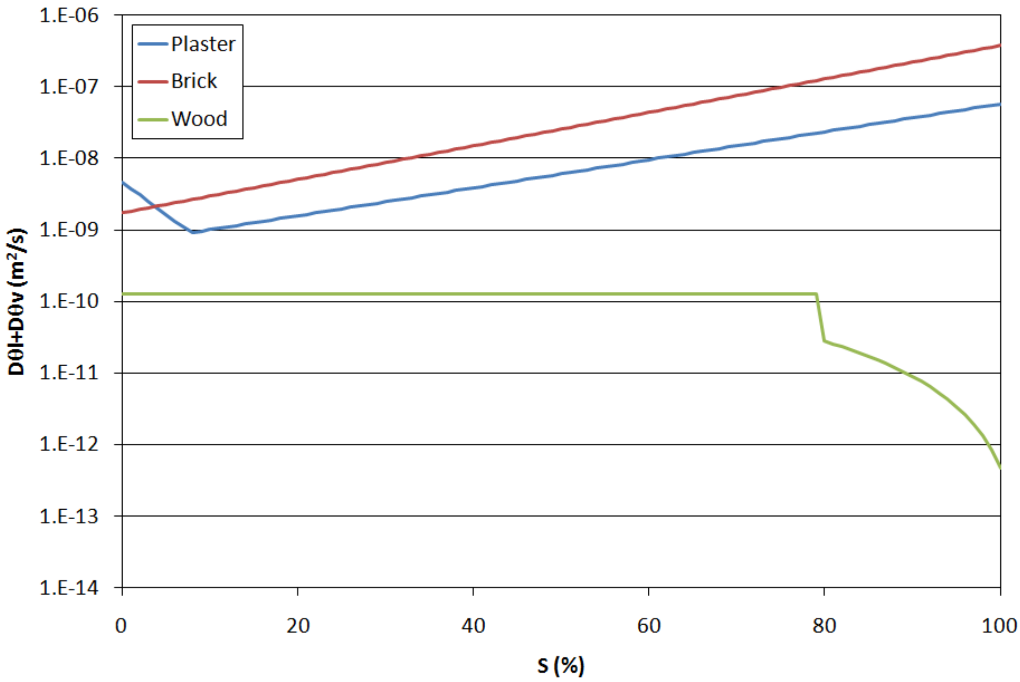


Figure 2-32: Coefficient of moisture transport associated with a moisture content gradient (liquid+vapor) versus saturation.

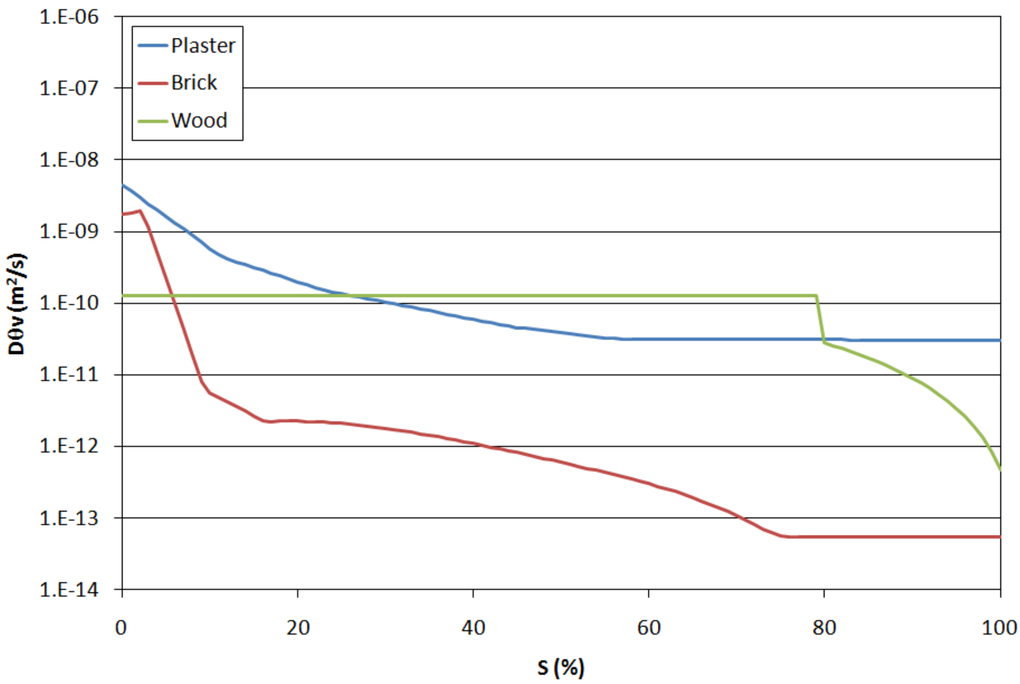


Figure 2-33: Coefficient of moisture transport associated with a moisture content gradient (vapor only) versus saturation.

### 2.4.2 Simulation parameters

The MBV-PUCPR experiment has been simulated reproducing the 8 $m^3$ cubic cell with a ventilation air renewal of 2.5 ACH. The temperature and relative humidity of the ventilated air measured during the experiment have been imposed in the simulation by creating a dedicated weather file. The simulated material has been exposed to all internal surfaces. Convective heat transfer coefficients have been imposed to 3.0 $W/m^2.K$ (common value of indoor environments). External convective moisture coefficient is null to account for the external vapor barrier. The discretization of the simulated materials, each finite volume has a maximal dimension of 1cm. Initial temperature and relative humidity for both air and material have been set to 23°C and 50 % respectively. A time step of 1 minute has been used for all simulations. Additional simulations showed that smaller finite volume size and/or smaller time step does not change the results significantly. The duration of the simulation represents about 5 days and corresponds to 5 cycles of ventilated air high/low humidity levels.

### 2.4.3 DOMUS Results

For each simulated material, a parametric study varying the internal convective moisture coefficient ($h_m$) has been performed to find the best match of the MBV value for the last 3 high/low humidity cycles of the experiment. Table 2-3 presents the values of $h_m$ and MBV that best fit the experimental MBV values and Figure 2-34 illustrates the variation of the vapor flux between the room air and the simulated material (Wood is chosen here as an example). The obtained $h_m$ are surprisingly very low. They actually are one order of magnitude lower than the usual value of $2.56\times10^{-3}$ m/s (EN ISO 15026, 2007). This discrepancy can originate from the fact that DOMUS considers one unique averaged sorption isotherm instead of taking into account the hysteresis that exists between the adsorption and desorption processes. Figure 2-35 shows the absolute humidity variation in the different experimental zones and obtained by DOMUS.

As can be seen, the higher peak is well represented by DOMUS. However, the minimal value is clearly overestimated. This discrepancy can be induced by an overestimation of the material desorption process that would induced a higher humidity level in the room air. Another possible explanation is that only a portion of the total exposed material surface area actually exchanges moisture with the room air. As presented in Figure 2-36, CFD simulation of the present problem (RANS k-$\omega$ model with high-resolution scheme, root mean square residuals lower than $10^{-6}$) shows that the air velocity close to the surface is very low, almost null for the major part of the exposed material surface leading to stagnation zone where almost no exchange occurs between the material and the surrounding air. Of course, the observed discrepancy can originate from both hypotheses.

Figure 2-37 and Figure 2-38 present the variations of the temperature and relative humidity measured in the different zones and obtained by DOMUS. As observed, there is a good agreement between the measurements and DOMUS predictions even if, because of the nodal (i.e. one unique zone) approach used in DOMUS, the heterogeneity of 3°C and 10%RH monitored during the experiment cannot be reproduced.

Table 2-3: Moisture Buffer Value.

| | $h_m$ (m/s) | MBV ($kg/m^{-2}$.%RH) 1st cycle | MBV ($kg/m^{-2}$.%RH) 2nd cycle | MBV ($kg/m^{-2}$.%RH) 3rd cycle | MBV ($kg/m^{-2}$.%RH) Averaged |
|---|---|---|---|---|---|
| **Experiment** | - | $3.32\times10^{-4}$ | $3.38\times10^{-4}$ | $3.13\times10^{-4}$ | $3.28\times10^{-4}$ |
| **Plaster** | $2.10\times10^{-4}$ | $3.36\times10^{-4}$ | $3.27\times10^{-4}$ | $3.14\times10^{-4}$ | $3.26\times10^{-4}$ |
| **Brick** | $1.90\times10^{-4}$ | $3.30\times10^{-4}$ | $3.28\times10^{-4}$ | $3.14\times10^{-4}$ | $3.24\times10^{-4}$ |
| **Wood** | $1.80\times10^{-4}$ | $3.35\times10^{-4}$ | $3.28\times10^{-4}$ | $3.13\times10^{-4}$ | $3.25\times10^{-4}$ |

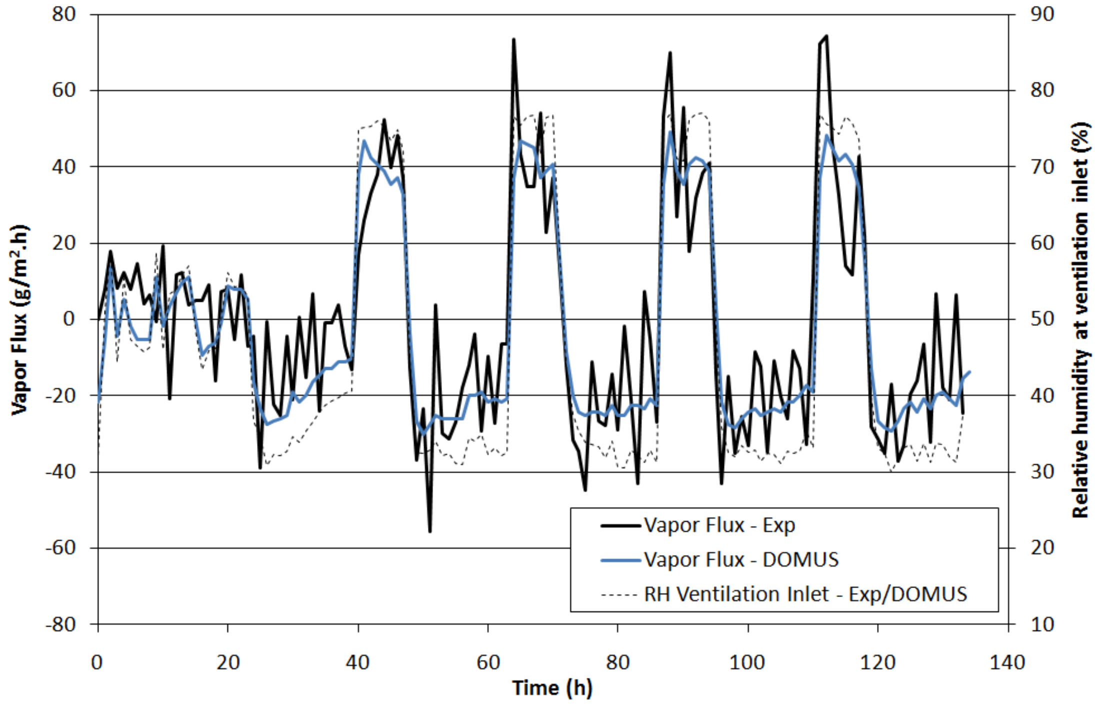


Figure 2-34: Vapor Flux between the room air and the tested material – Wood.

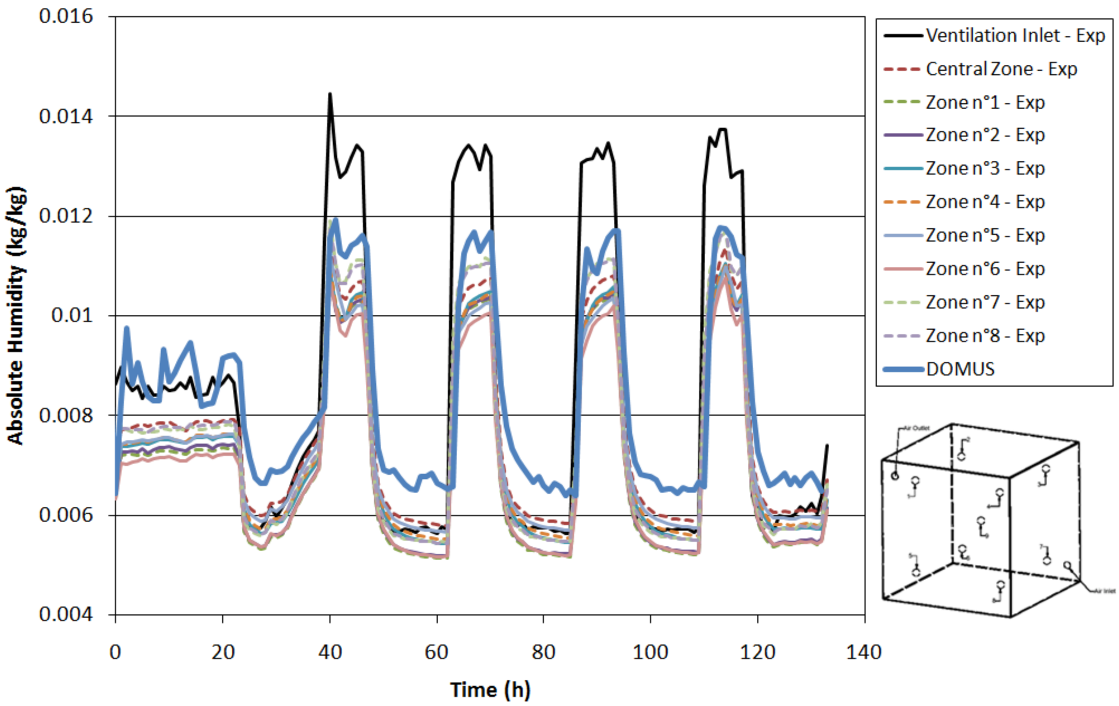


Figure 2-35: Absolute Humidity variation of the room air – Wood.

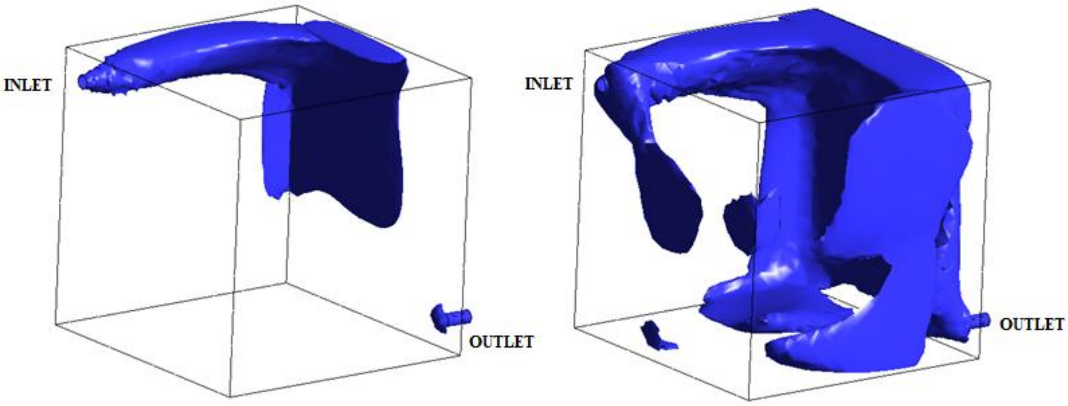


Figure 2-36: Region with air velocity higher than 0.1m/s (left) and 0.05m/s (right).

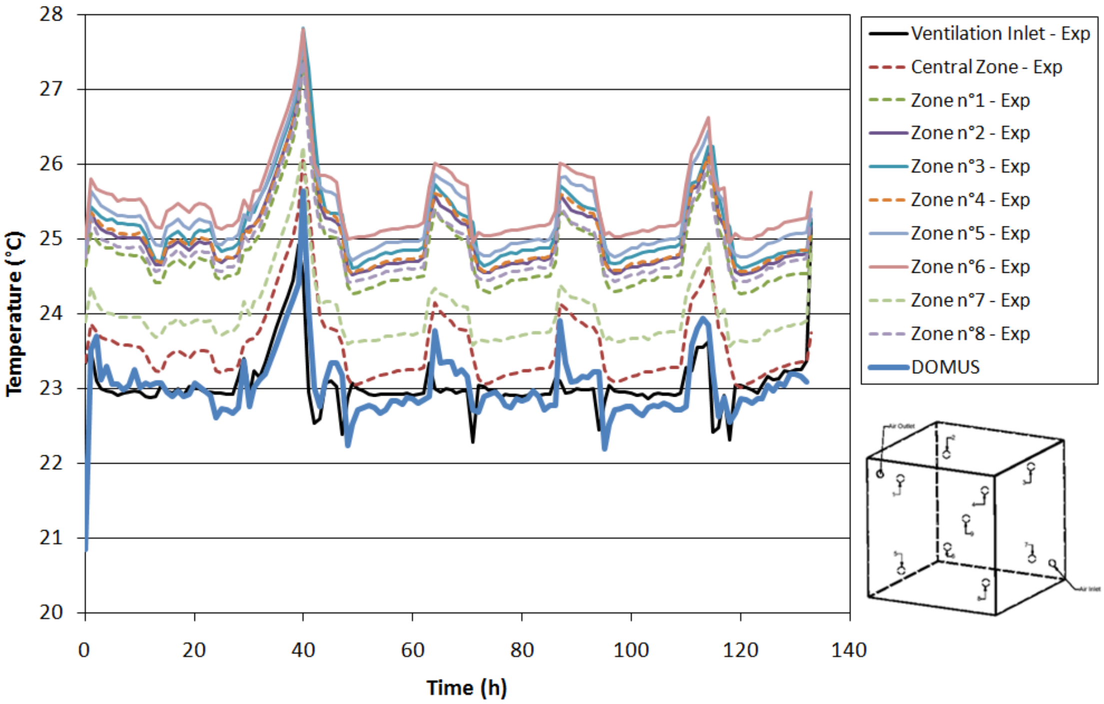


Figure 2-37: Temperature variation of the room air – Wood.

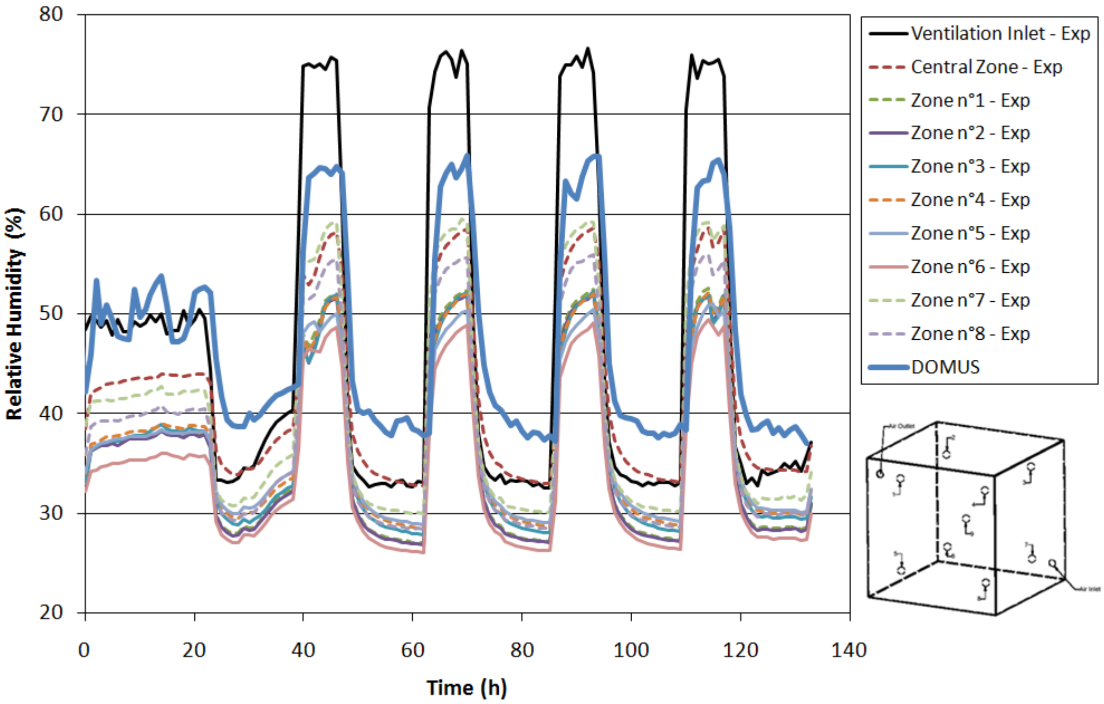


Figure 2-38: Relative Humidity variation of the room air – Wood.

### 2.4.4 Conclusion

The present validation aimed at showing the capabilities of DOMUS to account for the effect of porous materials that can be found in indoors spaces on the level of relative humidity of the room air. Considering the numerous uncertainties regarding the precise definition of the problem needed to simulate this case, such as the unknown material properties and convective mass transfer coefficient and the heterogeneity of the temperature and relative humidity within the room, DOMUS predictions are in good agreement with the measurements.

## 2.5 CP – Pressure Coefficient Evaluation

### 2.5.1 Verification of the implementation of CPCALC+ algorithm in DOMUS

The following graphs present a comparison between the original developments made by Grosso *et al.* (1995) (plain lines) and the results obtained by DOMUS (doted lines). The verification concerns the:

1. Reference Cp centerline profiles of the Windward wall,
2. Reference Cp centerline profiles of the Leeward wall,
3. Cp correction for boundary layer profile for the Windward wall,
4. Cp correction for the Surrounding Area Density for the Windward wall,
5. Cp correction for the Frontal Aspect Ratio for the Windward wall and
6. Cp correction for the Horizontal Distribution in relation to the Wind Angle for the Windward wall.

The CPCALC+ results have been extracted from the original document that presents figures of poor quality so that most of the small differences that are observed between CPCALC+ and DOMUS in this section are a direct consequence of those approximations. The only observed real discrepancy concerns the "Cp correction for the Surrounding Area Density for the Windward wall" case (Figure 2-42) for which DOMUS tends to slightly underestimate the value of the Cp correction. The coefficients of the algorithm have been checked; the source of the difference has not been discovered.

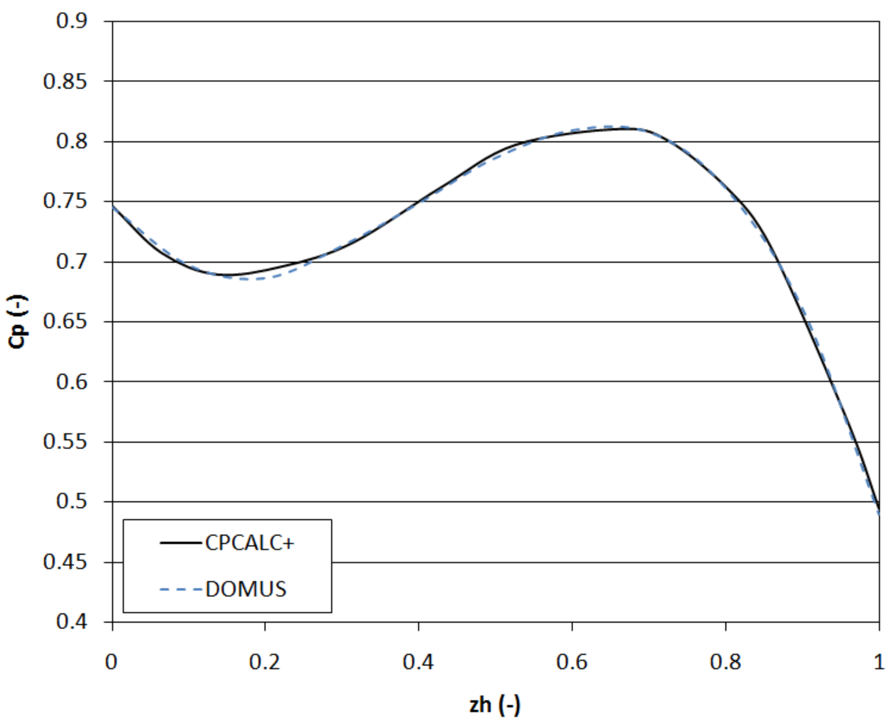


Figure 2-39: Reference Cp centerline profiles – Windward wall.

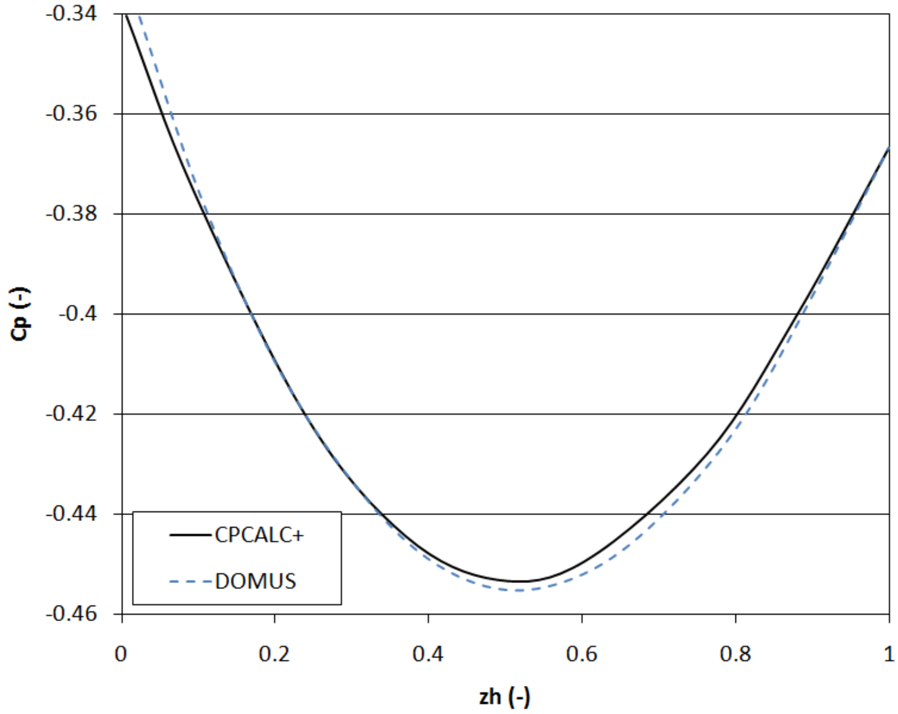


Figure 2-40: Reference Cp centerline profiles – Leeward wall.

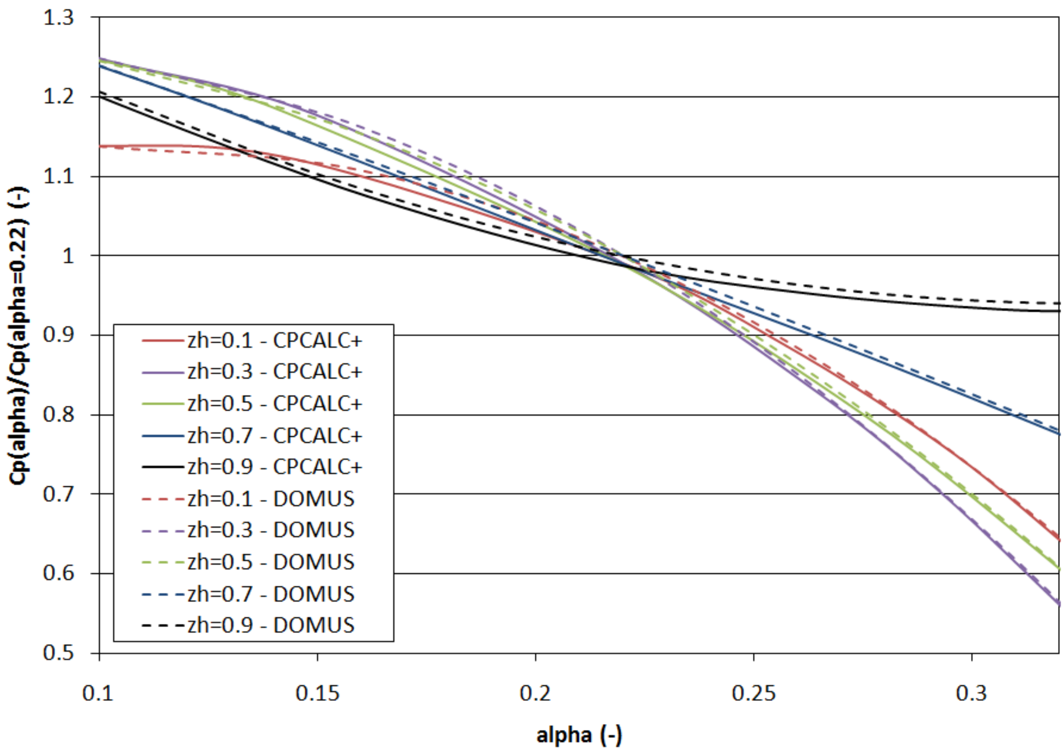


Figure 2-41: Cp correction for boundary layer profile (alpha) – Windward wall.

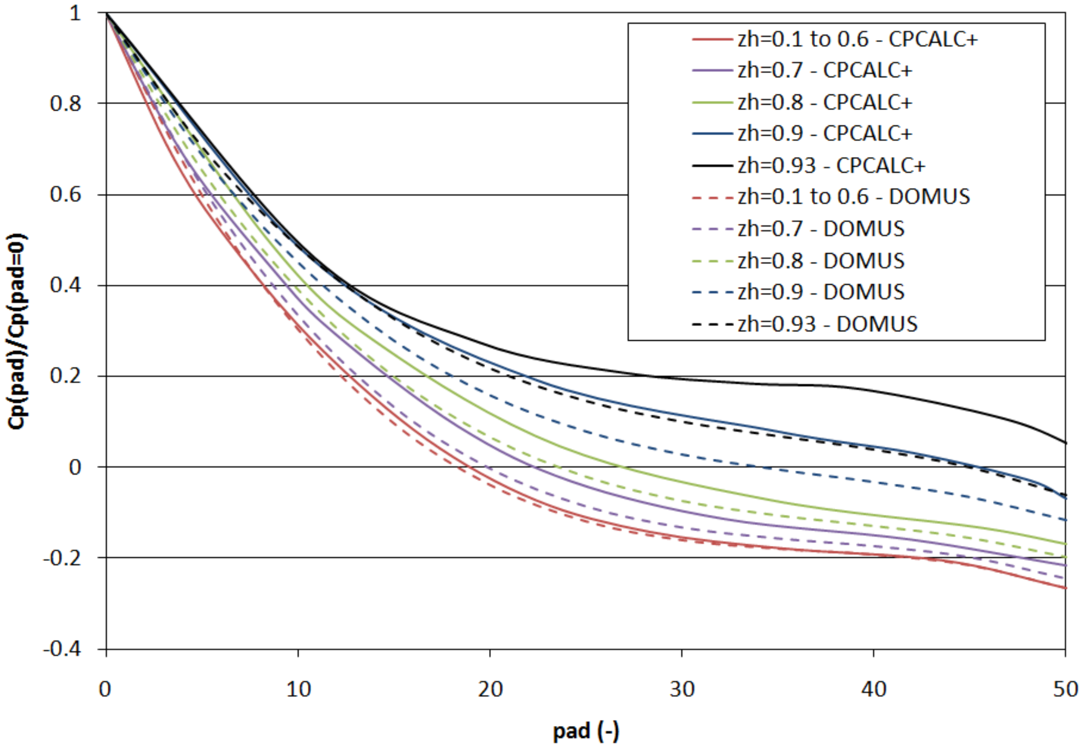


Figure 2-42: Cp correction for the Surrounding Area Density (pad) – Windward wall.

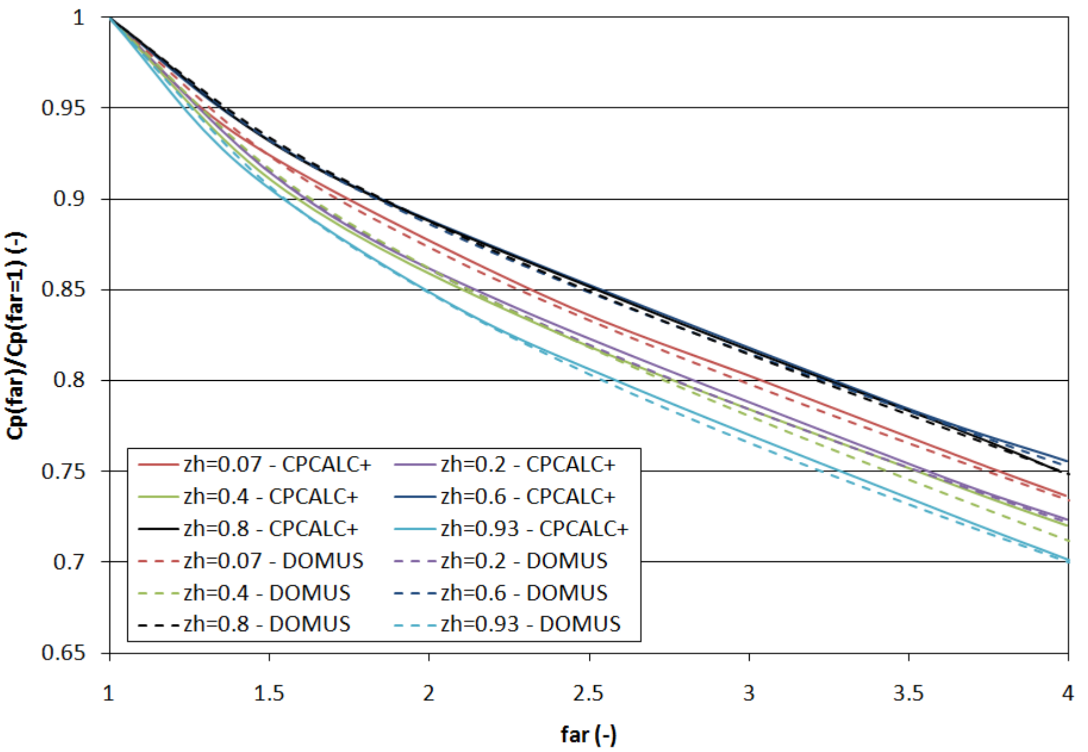


Figure 2-43: Cp correction for the Frontal Aspect Ratio (far) – Windward wall.

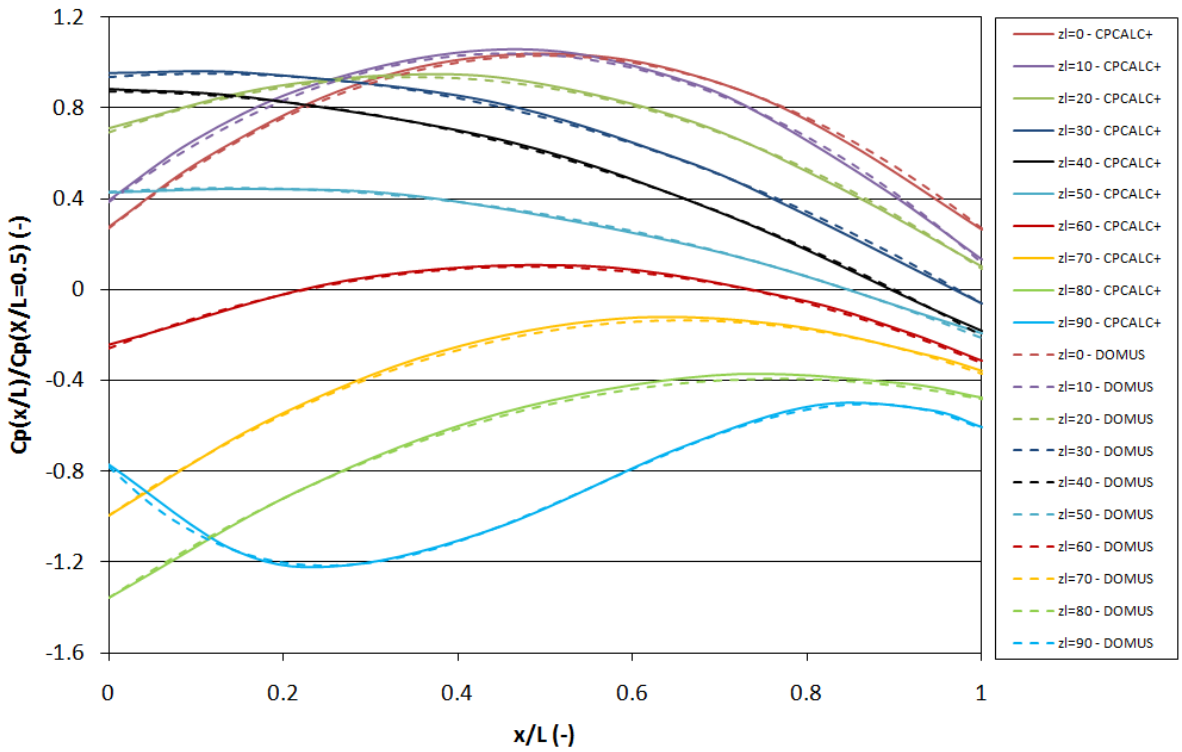


Figure 2-44: Cp correction for the Horizontal Distribution in relation to the Wind Angle (zl in °) – Windward wall.

### 2.5.2 Validation n°1

This section concerns the validation of DOMUS for low-rise parallelepiped building for which the Cp values have been obtained by measurement and by the use of the CPCALC+ program (Wong and Chin, 2002). Additional calculations have been performed with the Building Energy Simulation program ESP-r (ESRU, 2002) that includes the CPCALC+ algorithm.

Figure 2-45 to Figure 2-47 present the results obtained for wind to wall angle of 0°, 45° and 90°. First, for angles included in the original CPCALC+ dataset (i.e. 0° and 90°), DOMUS gives the same results as that of CPCALC+ and ESP-r. For angles not included in the dataset (45° where CPCALC+ data are only available for 40° and 50°), results differ only for the leeward wall. After investigation, CPCALC+ uses the nearest value (40° for 42°, 50° for 45° and 47°) and ESP-r uses the nearest higher value (always 50° for 45°) for windward wall. For leeward wall, the nearest higher value is used by both algorithms. Linear approximation I sued instead in DOMUS for both windward and leeward walls. The results obtained in this case with DOMUS are more in line with the experimental data.

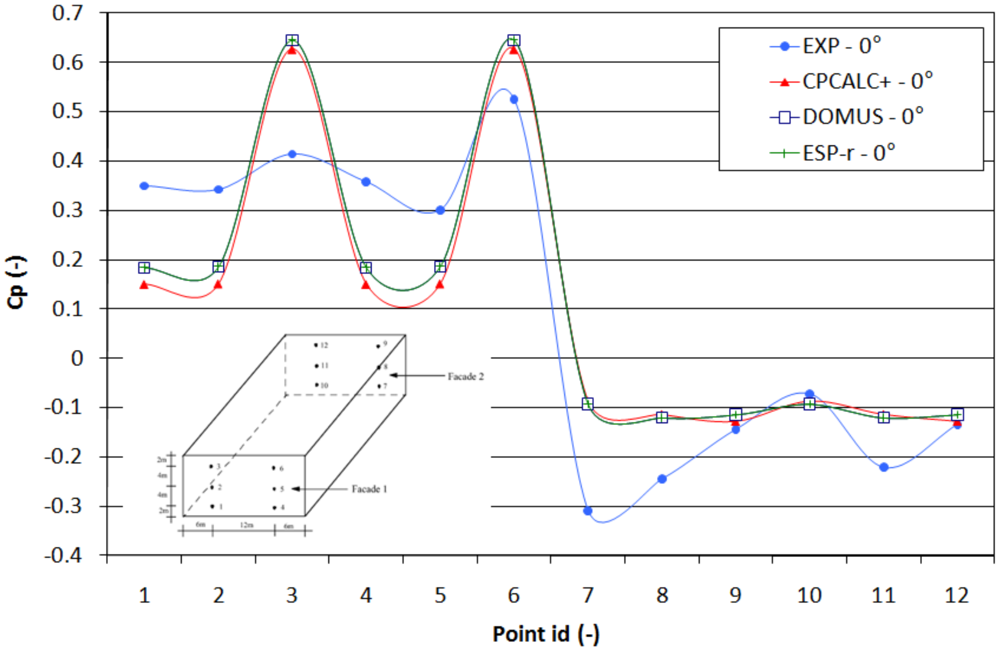


Figure 2-45: Cp values for wind to wall angle of 0°.

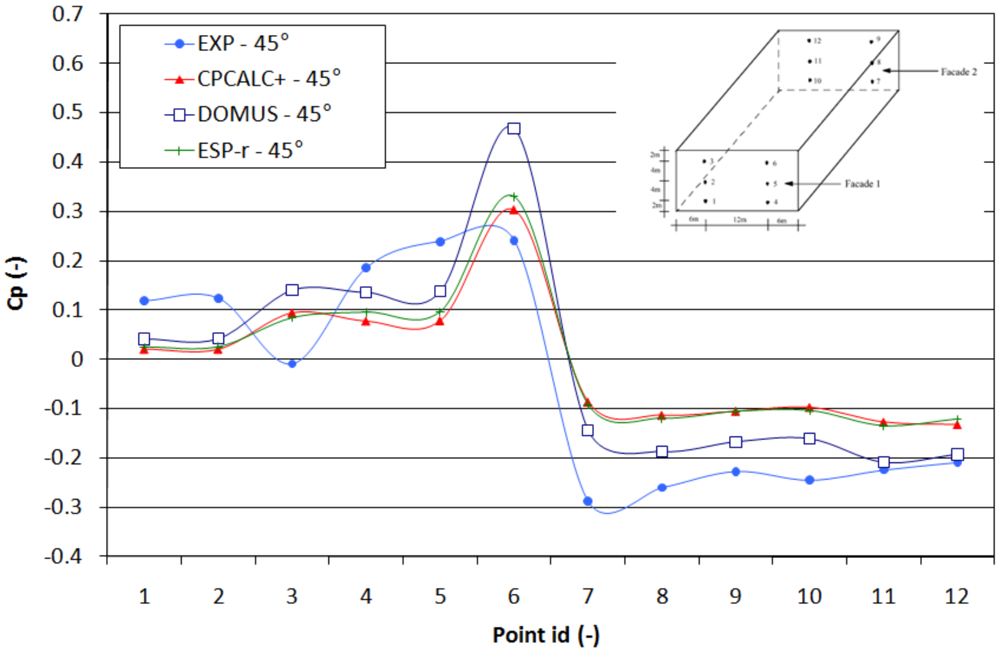


Figure 2-46: Cp values for wind to wall angle of 45°.

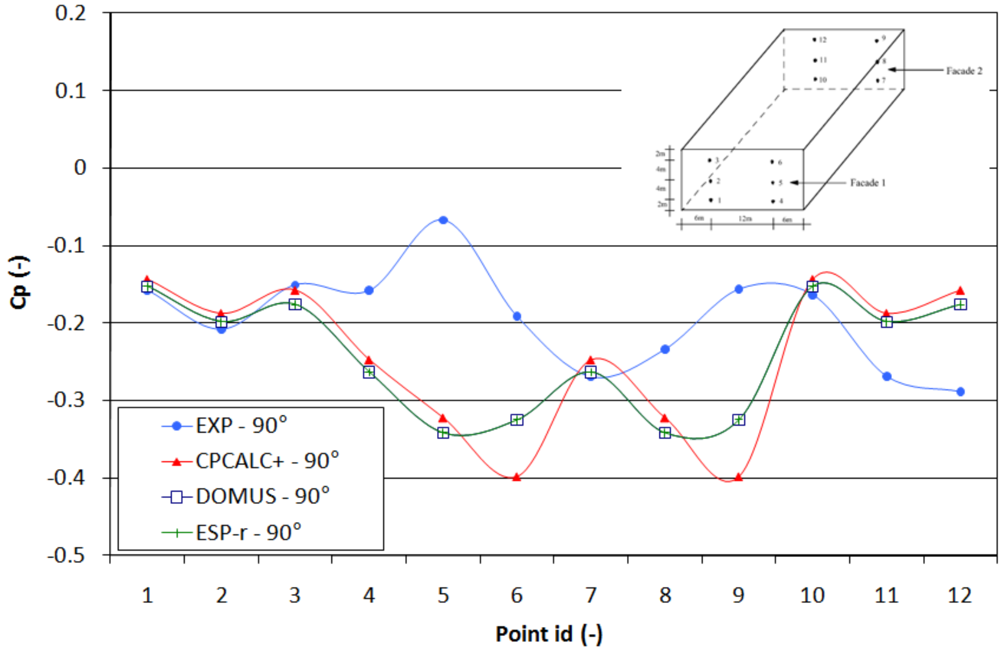


Figure 2-47: Cp values for wind to wall angle of 90°.

### 2.5.3 Validation n°2

This section concerns the second validation that has been performed comparing the Cp variation on different wall for three building shapes: a cube, a tall building, and a low building with large footprint. Comparisons were made with the wind tunnel data of Baines (1963) for a cubical building and a tall building with dimensions of 1:1:8 (length, width, height).

Figure 2-48 to Figure 2-50 present the results for the cubical, tall and low-flat buildings, respectively. The environmental parameters used here are: alpha=0.25, pad=0 and sbh=H (H=building height).

In the case of a cubical building for normal wind (Figure 2-48), both the front and side wall Cp values are very well predicted. The model predicts higher values for the leeward wall (+40%). With a 45° wind-to-wall angle, results are less precise.

In the case of a tall building (Figure 2-49), only the windward wall Cp coefficients are predicted correctly both in value and location. For the leeward wall, Cp values are underestimated by a factor 2. The predicted values for the side wall are within a wider range but represent well the vertical distribution. Note that this building is normally out of the scope of the CPCALC+ model as it has a frontal and side aspect ratio of 1/8 <<< 1/2 that is the minimal value that was used to evaluate the CPCALC+ correlations.

To finish, same conclusions can be done about the predictions of DOMUS for the low-flat building than the cubical one (Figure 2-50).

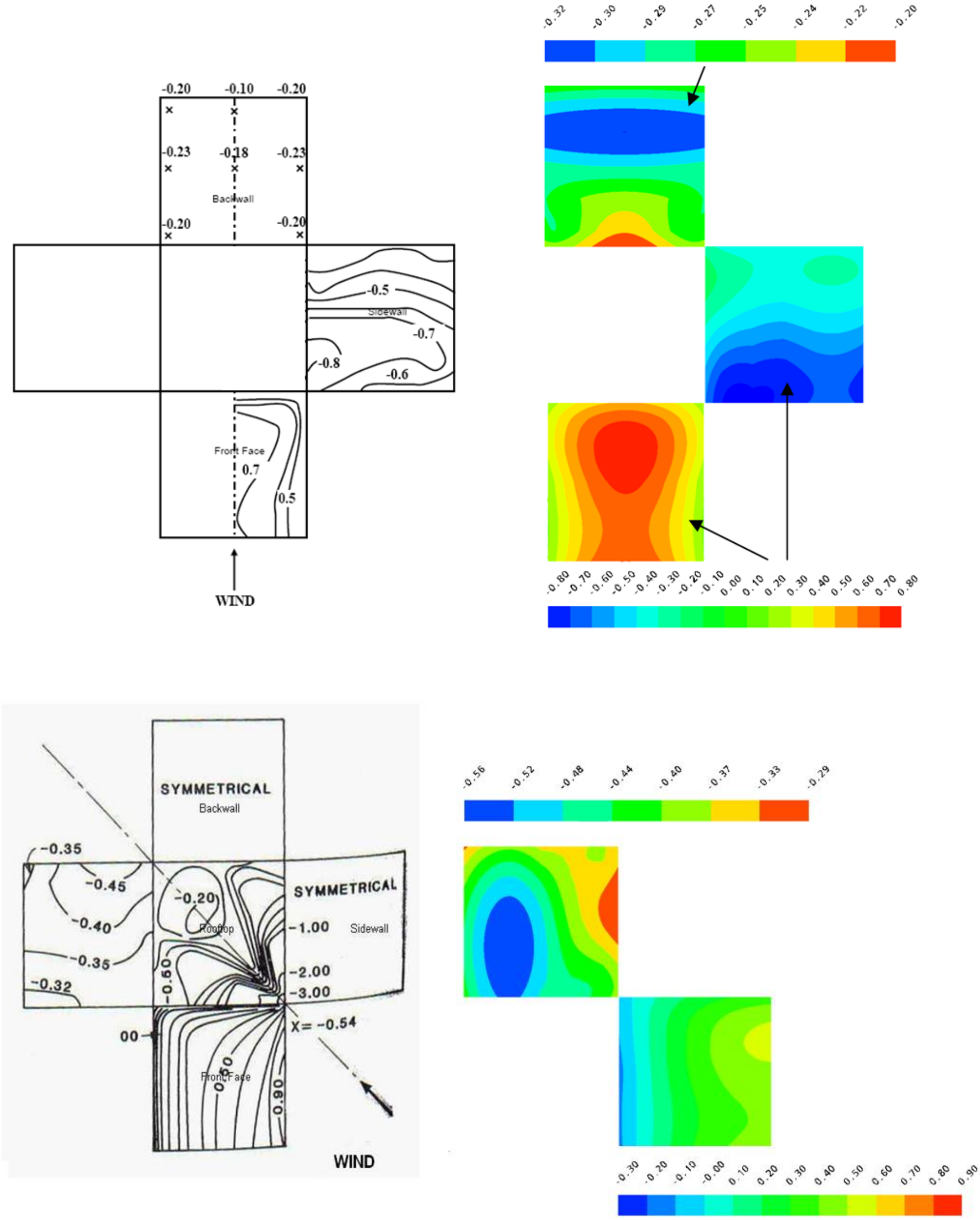


Figure 2-48: Wind-tunnel measurements (left) and present calculation (right) of the pressure coefficient on a cubical building for a shear inflow perpendicular to the building face (up) and with a 45° angle (down) after Baines (1963).

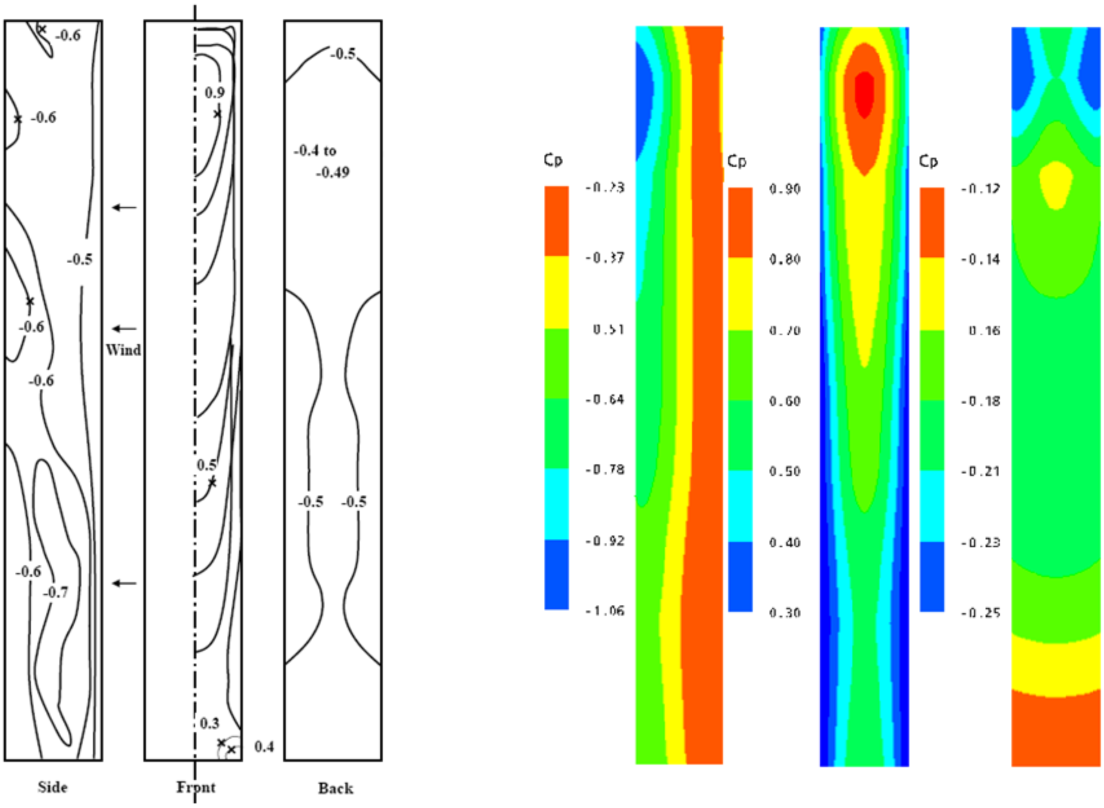


Figure 2-49: Wind-tunnel measurement after Baines (1963) (left) and present calculation (right) for a tall building for a shear inflow perpendicular to the building face (front).

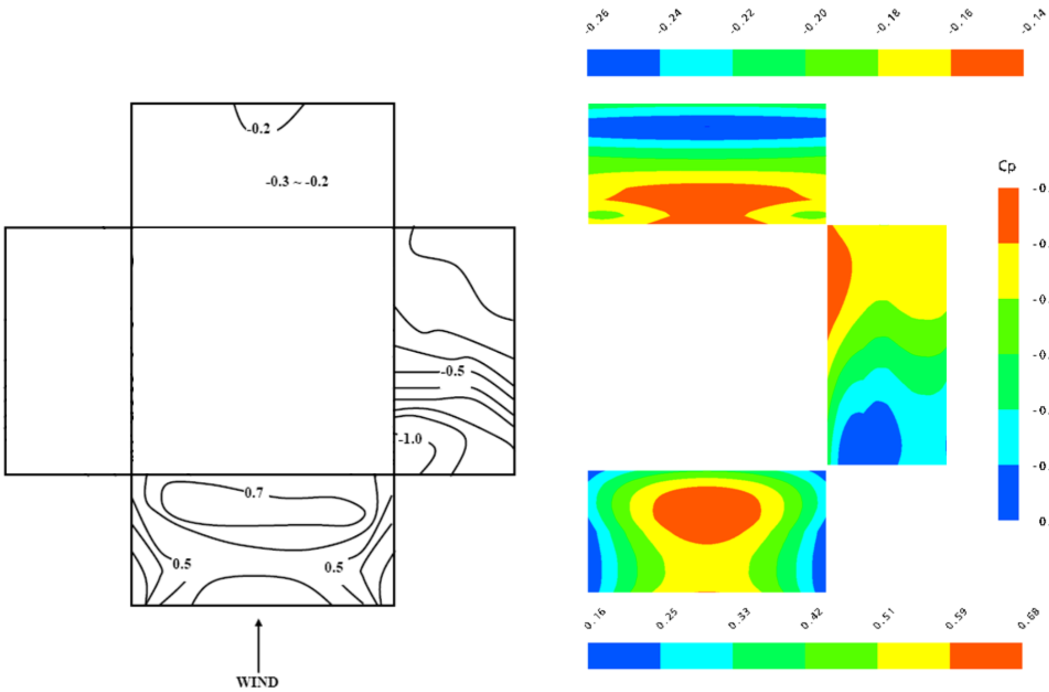


Figure 2-50: Wind-tunnel measurement after Baines (1963) (left) and present calculation (right) for a low-flat building for a shear inflow perpendicular to the building face (front).

### 2.5.4 Conclusion

Pressure coefficient calculation is required as a first step to evaluate airflows through cracks and large apertures in relation to infiltration and natural ventilation. The results presented here demonstrated on one hand the CPCALC+ algorithm has been successfully implemented in DOMUS. On the other hand, both validations show that good predictions are only obtained within the parameter ranges (Table 1-10) originally used to create the regressions.

## 2.6 NATVENT 1 – Wind-Tunnel Experiments

The building was designed with DOMUS in order to simulate the wind tunnel experiment. Because of the constant conditions as wind speed, wind incident angle and indoor and outdoor temperatures, specific weather files have been developed in order to reproduce the experiment conditions. The building structures designed in DOMUS are presented in Figure 1-12 (a) and (b).

### 2.6.1 Cross Ventilation

Figure 2-51 presents the results of wind tunnel cross ventilation experiments of Larsen (2006) and the predictions of the British Standards (1999) model implemented in DOMUS.

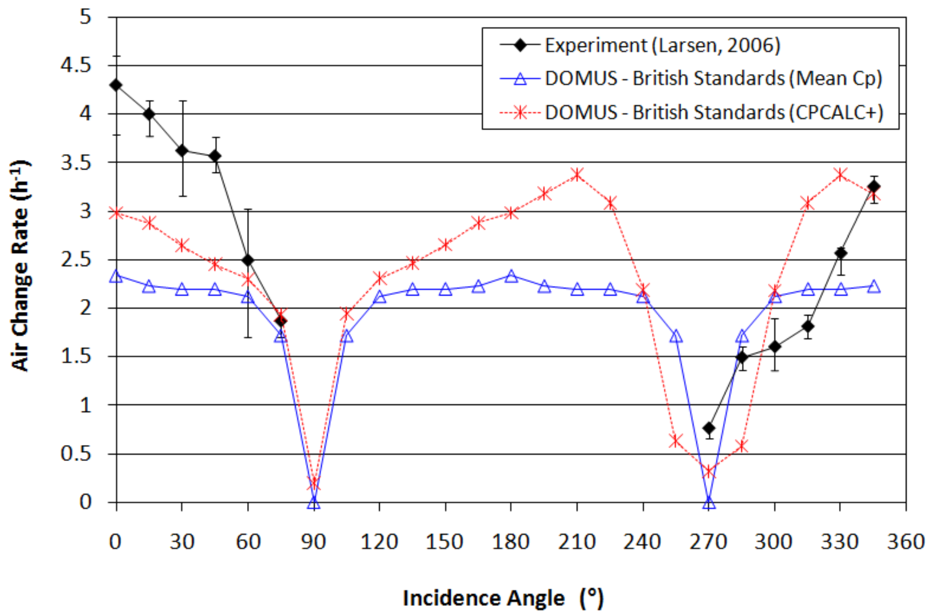


Figure 2-51: Comparisons between the experimental and DOMUS results performed for the wind tunnel - Cross Ventilation case.

Among the six different experiments (three different wind velocities and three distinct temperature differences) performed by Larsen (2006), only one is presented here (wind velocity of 1 m/s, isothermal case). In fact, the airflow rate is a linear function of the wind velocity so that results for other velocities can be easily interpolated from the presented ones. The experimental results clearly showed the linear behavior. Moreover, because of the fact that the openings are located at the same height, there is no thermal buoyancy effect; in this way, the negligible air change rate variations caused by temperature differences have not been treated in this case of high wind velocities. Results obtained by the model are the same for distinct temperature differences for the present configuration. The experimental results showed also that tendency with a slight variation probably due to the precision of the experimental measurements. The experimental results presented in Figure 2-51 are the airflow rate averages obtained from three distinct temperature differences results.

Results show that the British Standards (Mean CP) model, that is the Swami and Chandra (1988) model, is not capable of predicting the variation of the airflow rate according to the wind direction. The British Standards (CPCALC+) model tends to better follow this variation.

One particular drawback of the Mean CP-based model occurs when the wind is parallel to the openings. In this case, this model predicts no flow (the pressure coefficient difference between the openings is null) whereas the CPCALC+-based model is able to detect a small but notable airflow. However, it can be seen that the two models present almost the same mean relative difference of about 30% considering the whole set of data (Table 2-4).

Table 2-4: Relative differences (%) for the wind tunnel experiment - Cross Ventilation case.

| Model | Relative Difference (%) |
| --- | --- |
| DOMUS – British Standards (Mean CP) | 32.46 |
| DOMUS – British Standards (CPCALC+) | 31.11 |

### 2.6.2 Single-sided Ventilation

In order to illustrate the behavior of each single-sided ventilation model and to analyze the effect from different wind speeds (1, 3 and 5 m/s), temperature differences (0, 5 and 10°C) and incidence angles (varying from 0 to 345°) on the airflow rate. A total of 27 simulations using DOMUS has been performed. For the pressure coefficient calculation through the Mean CP method a wind exponent of 0.10 has been adopted, which is the value when there are no obstructions affecting the wind. For the CPCALC+ method, the same value has been used and for the plan area density and surrounding building height the values of pad = sbh = 0 have been adopted because there are no obstructions inside the wind tunnel.

The results, presented in Figure 2-52 to Figure 2-54, represent the air change rates as a function of the incidence angle and the temperature difference of 5°C. Each line represents one of the selected wind speeds. As the wind angle dependency is not included in the de Gids and Phaff (1982) model, a constant air flow rate is obtained for each wind speed. On the other hand, Larsen's model does present the expected angular dependency.

The differences noticed between the Larsen (Mean CP) and Larsen (CPCALC+) models are caused by the calculation of the pressure coefficient. While the Mean CP method calculates the wall mean pressure coefficient, the CPCALC+ method estimates the pressure coefficient value for the geometric center of the opening. As a consequence, the CP values calculated by the CPCALC+ method are higher when the wind incidents directly on the window (angle in the interval of $270° < \beta < 360°$) than for angles between $0° < \beta < 90°$. The Mean CP method is not able to represent this actual behavior.

The relative differences for the windward, leeward and parallel incidence angles have been presented in Table 2-5 and the relative differences calculations consider the three wind speed values (1, 3 and 5 m/s). It is noticed for the windward and leeward incidence angles, the Larsen's model by using the CPCALC+ calculation presents slightly better results than the two others. When the parallel incidence angle is analyzed, the Mean CP method has a difference higher than the others. This represents the model difficulty to calculate the pressure coefficient in angles near 90°.

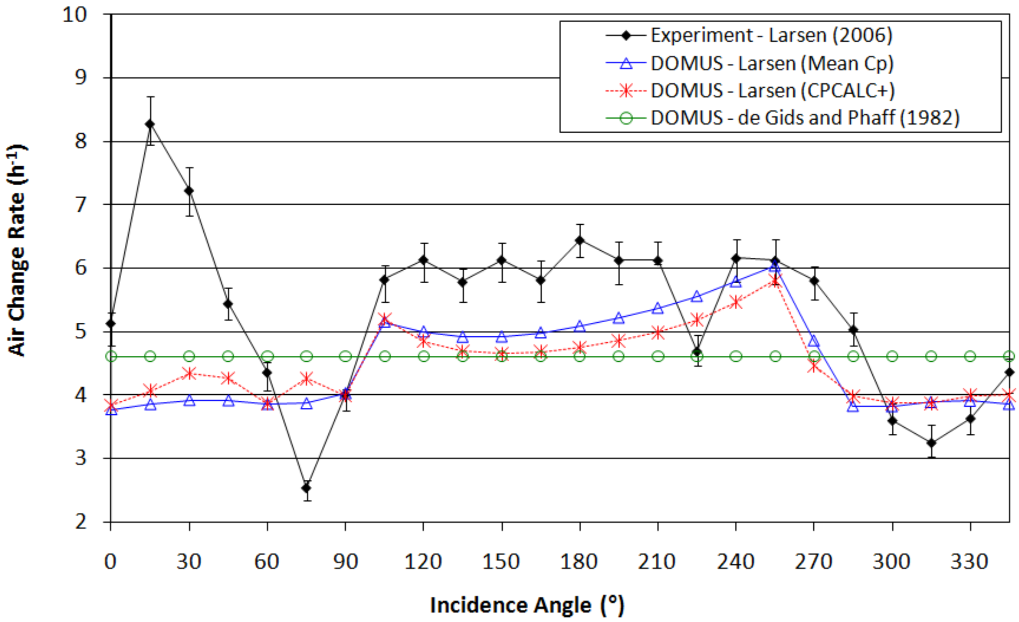


Figure 2-52: Comparisons between the experimental and DOMUS results for the wind tunnel case with wind speed of 1 m/s – Single-sided ventilation case.

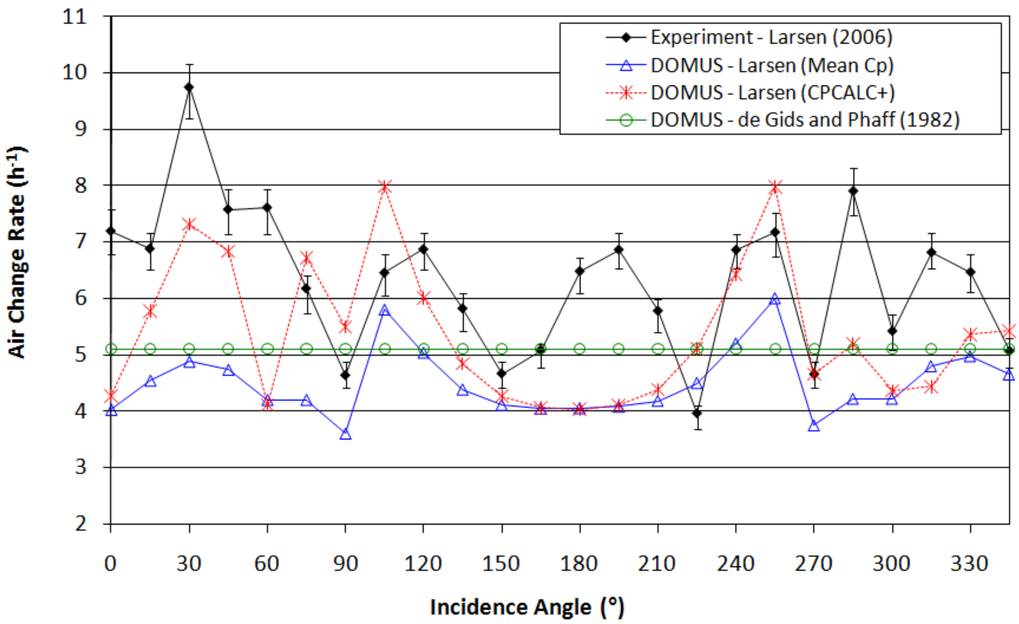


Figure 2-53: Comparisons between the experimental and DOMUS results for the wind tunnel case with wind speed of 3 m/s – Single-sided ventilation case.

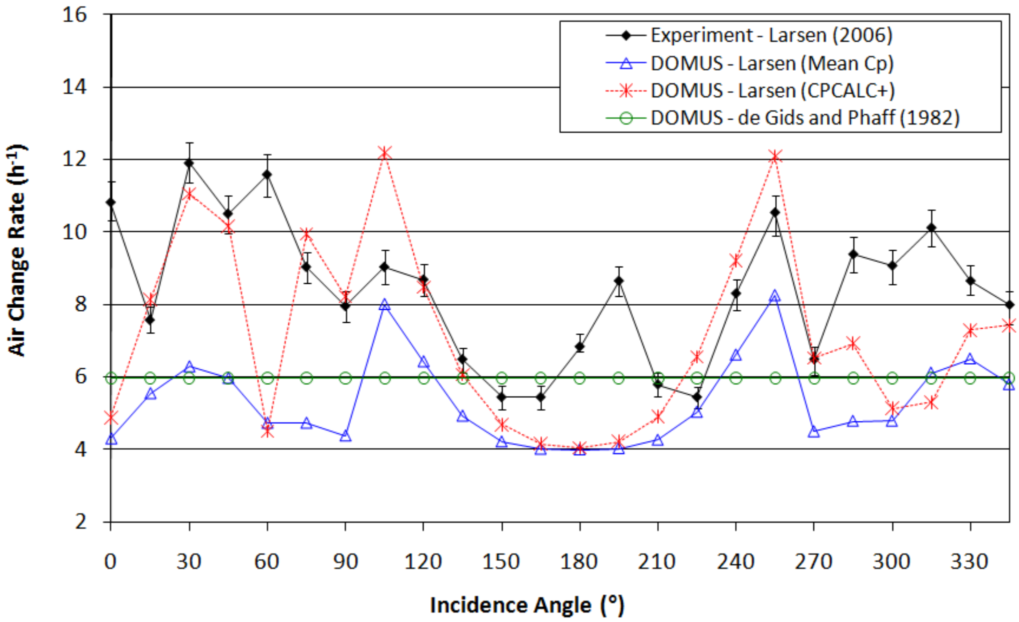


Figure 2-54: Comparisons between the experimental and DOMUS results for the wind tunnel case with wind speed of 5 m/s – Single-sided ventilation case.

Table 2-5: Relative differences (%) for the wind tunnel experiment - Single-sided ventilation case.

| Model | Windward | Leeward | Parallel |
|---|---|---|---|
| DOMUS – Larsen (Mean CP) | 34.25 | 20.85 | 22.38 |
| DOMUS – Larsen (CPCALC+) | 24.99 | 19.75 | 7.68 |
| DOMUS – de Gids and Phaff (1982) | 29.89 | 20.39 | 14.68 |

### 2.6.3 Conclusion

The validation against the wind-tunnel experiments showed that the use of the Larsen (CPCALC+) model actually improves the predictions, particularly in the case of single-sided configurations.

## 2.7 NATVENT 2 – On-Site Experiment

### 2.7.1 DOMUS Results

The comparisons of the on-site experiment and DOMUS are compared in this section. According to Dascalaki *et al.* (1999), the building is located in an open urban environment on top of a hill across from the Acropolis of Athens, consequently, a wind exponent of 0.28 has been chosen for the pressure coefficient calculation by the Mean CP and CPCALC+ methods. For the last one, the pad = sbh = 0 have also been used. Figure 2-55 shows the comparisons between the simulation and the measured results. According to those results, it has been noticed that the Larsen model using the CPCALC+ method to calculate the pressure coefficient has provided air flow rates most in line with the experimental ones. When the relative differences for all the obtained results are calculated, the previous graphical observation is verified (Table 2-6).

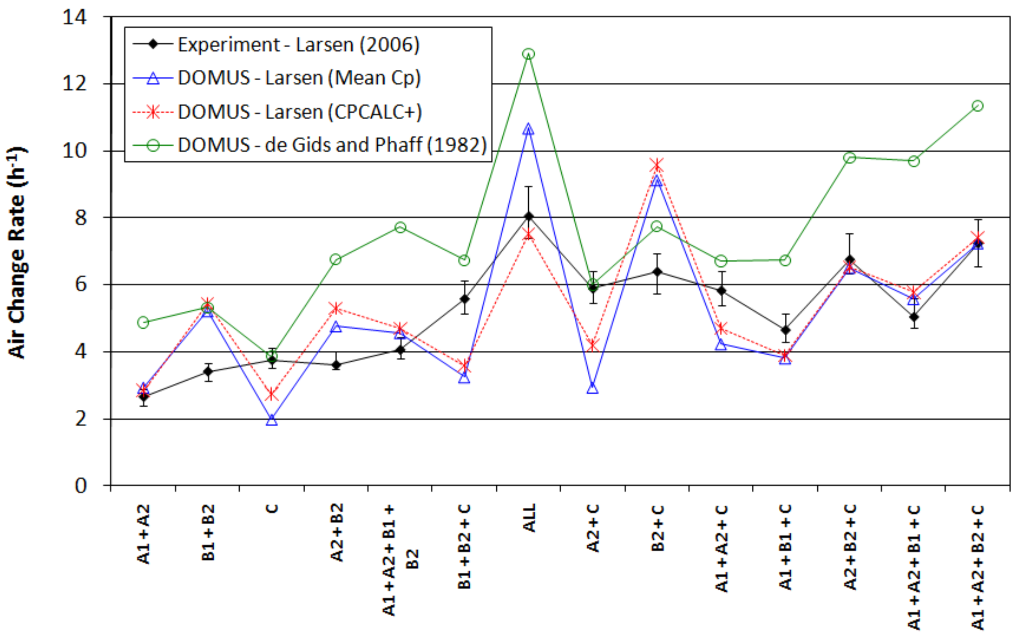


Figure 2-55: Comparisons between the experimental and DOMUS results for the NOA Building case.

It should be noticed that the wind incidence angle varied around 90° during the experiments for which Larsen model already showed better prediction to reproduce the results obtained in the wind tunnel experiment. The slightly better results of Larsen (CPCALC+) compared to Mean CP essentially occur for 3 points (C, All, A2 + C) where the angle is about 70° for which this model showed also better prediction in the wind tunnel experiment. On the other side, the de Gids and Phaff (1982) model, which presented good predictions for the wind tunnel experiment, was not capable of providing good results in this case.

Table 2-6: Relative differences (%) for the NOA Building experiment.

| Model | Relative Difference (%) |
|---|---|

| | |
|---|---|
| DOMUS – Larsen (Mean CP) | 27.71 |
| DOMUS – Larsen (CPCALC+) | 24.03 |
| DOMUS – de Gids and Phaff (1982) | 49.06 |

### 2.7.2 Conclusion

The validation against the on-site experiment showed that the use of the Larsen (CPCALC+) model actually improves the predictions.

# 3 CONCLUSION

This report describes the additional validations and verifications performed to test the capabilities of DOMUS to treat heat and mass transfer problems not covered by ASHRAE 1052 – RP Toolkit "Building Fabric Analytical Tests" nor ANSI/ASHRAE Standard 140 – 2007 titled Standard Method of Test for the Evaluation of Building Energy Analysis Computer Programs.

The first part of the report is dedicated to the simulation of moisture transfer. The proposed verification/validation problems have been chosen to gradually increase the complexity of the heat and moisture transfers that take place between the porous material and the surrounding air. The first case (HAMSTAD – Analytical Benchmark n°2) that was dedicated to transient vapor transfer into a porous material under isothermal condition validates the capabilities of DOMUS to solve the transport of vapor due to local moisture content gradient into the material. The second case (ANNEX 41 Subtask 1 – Common Exercise 1) helps verifying the treatment of the moisture mass conservation into the zone air (case 1A) and the vapor transfer between the porous material and the zone air i.e. the transport into the material and the transfer at the material surface (case 1B). By simulating an in-situ experimental facility (ANNEX 41 Subtask 1 – Common Exercise 3), DOMUS has been validated to predict the variations of relative humidity and heating energy taking into account the whole complexity (climatic solicitations, presence of heat and moisture production, moisture buffering effect of the porous envelop) of real buildings. Another step of complexity has been added with the last case (MBV-PUCPR) for which a strong three-dimensional heterogeneity of the indoor airflow has been imposed. For this case, in front of several uncertainties, it was only possible to perform parametric study in order to reproduce the trends observed in the experiment. Note that, because of the 3D heterogeneity of the local variables, DOMUS that is based on the well-mixed assumption (nodal model) should be coupled with other modeling approach such as CFD or Zonal models.

The second part of the report aims at validating the capabilities of DOMUS in modeling natural ventilation through large apertures such as open windows and doors. The first case (CP – Pressure Coefficient Evaluation) concerns the verification of the implementation of the CPCALC+ algorithm, important step as wind effect on naturally induced airflows in buildings rely on the good prediction of the coefficient of pressure (CP). Additionally to the original CPCALC+ validation data, several cases have been simulated to evaluate the potential and limitation of the algorithm. The second and third cases (NATVENT 1 and 2) permit to test the capabilities of the different empirical models that have been implemented in DOMUS to calculate the airflow through open windows and doors. Results show that the newest model of Larsen (2006) coupled with the CPCALC+ algorithm provides the best predictions for both wind-tunnel and on-site experiments.

The perspective of the present work essentially lies on the implementation of a dedicated airflow network algorithm in DOMUS to calculate in an automatic way the airflows between the different rooms of a building. Note that the verification of the implementation of the CPCALC+ algorithm has already been a first important step in this direction.

# 4 ACKNOWLEDGEMENT

The author wants to thank Dr. Roberto Zanetti Freire, Lecturer at Pontifícia Universidade Católica do Paraná – PUCPR, for providing the results of NATVENT 1 and 2 cases and Luiz Ricardo Akihito Abe, student at the Mechanical Engineering Department of Pontifícia Universidade Católica do Paraná – PUCPR, for his work regarding the MBV-PUCPR validation.

# 5 REFERENCES

Abadie M.O., Mendes N. 2006a. Comparative Analysis between Response-Factor and Finite-Volume based Methods for predicting Heat and Moisture Transfer through Porous Building Materials. Journal of Building Physics, London - UK, 30, pp. 7-37.

Abadie M.O., Mendes N. 2006b. Is the Vapor Diffusion Thickness (sd) of 0.15m appropriated for Common Exercise 3? In: 5th working meeting in IEA annex 41, 2006, Kyoto.

Atkins R.E., Cermak J.E. 1976. Wind Pressures on Buildings. CER 76-77REA-JEC15, Fluid Dynamics and Diffusion Laboratory, Colorado State University, CO.

Baines WD. 1963. Effects of Velocity Distribution on Wind Loads and Flow Patterns on Buildings. Symposium on wind effects on buildings and structure, Middlesex, England, National Physical Lab. 1, pp. 197-225.

Bednar T., Hagentoft C.-E. 2005. Analytical Solution for Moisture Buffering Effect - Validation Exercises for Simulation Tools, 7$^{th}$ Nordic Symposium on Building Physics, Reykjavik, June.

British Standards. 1999. Code of Practice for Design of Buildings: Ventilation Principles and Designing for Natural Ventilation, 1 edition, British Standards Institution, BS5925.

de Gids W., Phaff H. 1982. Ventilation Rates and Energy Consumption due to Open Windows: a Brief Overview of Research in the Netherlands. Proceedings of the 3$^{rd}$ International Energy Agency, Air Infiltration Center Conference, 1, pp. 4-5.

EN ISO 15026. 2007. Hygrothermal performance of building components and building elements – assessment of moisture transfer by numerical simulation. Geneva: International Standards Organisation.

ESRU. 2002. The ESP-r System for Building Energy Simulation. User Guide Version 10 Series, University of Strathclyde, Glasgow, Scotland.

Feustel H.E., Rayner-Hooson A. 1990. Fundamentals of the Multizone Air Flow Model – COMIS. International Energy Agency - Air Infiltration and Ventilation Centre, Technical Note AIVC 29, Coventry, Great Britain.

Freire R.Z. 2010. Numerical Simulation of Photovoltaic Hybrid Ventilation Systems Combined with a Whole-Building Hygrothermal Model. PhD Dissertation, Pontifical Catholic University of Parana – PUCPR, May 7$^{th}$.

Grosso M. 1992. Wind Pressure Distribution around Buildings - a Parametrical Model. Energy and Building, 18(2), pp. 101-131.

Grosso M. 1993. Modelling Wind Pressure Distribution on Buildings for Passive Cooling. Proceedings of the International Conference Solar Energy in Architecture and Urban Planning, Commission of the European Communities, Florence, 17-21 May.

Grosso M., Marino D., Parisi E. 1994. Wind Pressure Distribution on Flat and Tilted Roofs: a Parametrical Model. Proceedings of the European Conference on Energy Performance and Indoor Climate in Buildings, Lyon, France, November 24-26.

Grosso M. 1995. CPCALC+ Calculation of Wind Pressure Coefficients on Buildings. PASCOOL Research Program Report, Turin, Italia.

Grosso M., D. Marino, E. Parisi. 1995. A Wind Pressure Distribution Calculation Program for Multizone Airflow Models. Building Simulation, Madison, Wisconsin, USA.

Hagentoft C.-E. 2002. HAMSTAD – Final report: Methodology of HAM-Modeling. Report R-02:8. Gothenburg, Department of Building Physics, Chalmers University of Technology.

Hussain M., Lee B.E. 1980. An Investigation of Wind Forces on Three-dimensional Roughness Elements in a Simulated Atmospheric Boundary Layer Flow. Report BS 55, Dept. Building Science, University of Sheffield.

IEA. 1996. International Energy Agency – Annex 23: Multizone Airflow Modelling - Evaluation of COMIS Appendices. Technical report, Swiss Federal Institute of Technology, Lausanne, LESO, Institute of Building Technology, Torino, Italy.

Larsen T.S. 2006. Natural Ventilation Driven by Wind and Temperature Difference. PhD thesis. Aalborg University, Aalborg, Denmark.

Larsen T.S., Heiselberg P. 2008. Single-sided Natural Ventilation driven by Wind Pressure and Temperature Difference. Energy and Buildings, 40, pp. 1031-1040.

Lenz K., Holm A. 2005. Two Real Exposure Rooms at FhG. Annex 41 – Subtask 1 Common Exercise 3 (Whole building heat and moisture analysis).

Liddament M.W. 1986. Air Infiltration Calculation Techniques - an Applications Guide. Air Infiltration and Ventilation Centre, Bracknell, U.K.

Meissner J.W., Mendes N., Mendonça K.C., Moura L.M. 2010. A Full-Scale Experimental Set-up for Evaluating Moisture Buffer Effects of Porous Material. International Communications in Heat and Mass Transfer, 37, pp. 1197-1202.

Mendes N., Lamberts R., Philippi P.C. 2002a. Conducción Sensíble y Latente en Paredes Porosas de Edificaciones, Submetidas a Altos Gradientes de Temperatura y Humedad. Revista de la Construcción, 1, pp. 31-36.

Mendes N., Philippi P.C., Lamberts R. 2002b. A New Mathematical Method to Solve Highly-Coupled Equations of Heat and Mass Transfer. International Journal of Heat and Mass Transfer, 45, pp. 509-518.

Mendes N., Ridley I., Lamberts R., Philippi P.C., Budag K. 1999. Umidus: A PC Program for the Prediction of Heat and Moisture Transfer in Porous Building Elements. Building Energy Simulation, 20(4), pp. 2-8.

Mendes N., Winkelmann F.C., Philippi P.C., Lamberts R. 2000. Cargas de Enfriamiento y Transferencia de Humedad atraves de Paredes Porosas: Sensibilidad al Tratamiento de Coeficientes de Transferencia en el Modelo de Philip y DeVries. Revista Información Tecnológica del Chile, 11, pp. 1-8.

Mendes N., Winkelmann F.C., Lamberts R., Philippi P.C. 2003. Moisture Effects on Conduction Loads. Energy and Buildings, 35(7), pp. 631-644.

Rode C. 2005. Moisture Buffering of Building Materials. Report BYG.DTU R-126, Department of Civil Engineering, Technical University of Denmark, Lyngby, Denmark.

Rode C., Peuhkuri R., Mortensen L.H. 2005. Moisture balance of BESTEST building. Annex 41 – Subtask 1 Common Exercise 1.

Santos G.H., Mendes N., Freire R.Z. 2003. Análise de Sensibilidade e de Performance Higrotérmica de Solos Insaturados. Revista de la Construcción, 2, pp. 50-56.

Swami M.V., Chandra S. 1988. Correlations for Pressure Distribution of Buildings and Calculation of Natural Ventilation Airflow. *ASHRAE Transactions,* 4(94), pp. 244-266.

Wong N.H., Chin H.K. 2002. An Evaluation Exercise of a Wind Pressure Distribution Model. Energy and Buildings, 34, pp. 291-309.